Evaluating models for lithospheric loss and intraplate volcanism beneath the Central Appalachian Mountains

Maureen D. Long[1*], Lara S. Wagner[2], Scott D. King[3], Rob L. Evans[4], Sarah E. Mazza[5], Joseph S. Byrnes[6,7], Elizabeth A. Johnson[8], Eric Kirby[9], Maximiliano J. Bezada[6], Esteban Gazel[10], Scott R. Miller[11], John C. Aragon[1,12], Shangxin Liu[3]

[1]Dept. Earth & Planetary Sciences, Yale University, New Haven, CT, USA
[2]Earth & Planets Laboratory, Carnegie Institution for Science, Washington, DC, USA
[3]Dept. Geosciences, Virginia Tech, Blacksburg, VA, USA
[4]Dept. Geology & Geophysics, WHOI, Woods Hole, MA, USA
[5]Dept. Geosciences, Smith College, Northampton, MA, USA
[6]Dept. Earth & Environmental Sciences, University of Minnesota, Minneapolis, MN, USA
[7]School of Earth & Sustainability, Northern Arizona University, Flagstaff, AZ, USA
[8]Dept. Geology & Environmental Science, James Madison University, Harrisonburg, VA, USA
[9]Dept. Geological Sciences, University of North Carolina at Chapel Hill, Chapel Hill, NC, USA
[10]Dept. Earth & Atmospheric Sciences, Cornell University, Ithaca, NY, USA
[11]Dept. Geology & Geophysics, University of Utah, Salt Lake City, UT, USA
[12]Now at: Earthquake Science Center, U.S. Geological Survey, Menlo Park, CA, USA
*Corresponding author. Email: maureen.long@yale.edu

Submitted to Journal of Geophysical Research, 6/7/21

Key Points

- There is a present-day geophysical anomaly in the upper mantle co-located with unusually young volcanism in the Central Appalachians.
- We synthesize constraints from geophysics, petrology/geochemistry, and geomorphology to constrain possible models for lithospheric loss.
- We favor one or more Rayleigh-Taylor lithospheric instabilities, perhaps in combination with shear-driven upwelling.

Abstract

The eastern margin of North America has been shaped by a series of tectonic events including the Paleozoic Appalachian Orogeny and the breakup of Pangea during the Mesozoic. For the past ~200 Ma, eastern North America has been a passive continental margin; however, there is evidence in the Central Appalachian Mountains for post-rifting modification of lithospheric structure. This evidence includes two co-located pulses of magmatism that post-date the rifting event (at 152 Ma and 47 Ma) along with low seismic velocities, high seismic attenuation, and high electrical conductivity in the upper mantle. Here, we synthesize and evaluate constraints on the lithospheric evolution of the Central Appalachian Mountains. These include tomographic imaging of seismic velocities, seismic and electrical conductivity imaging along the MAGIC array, gravity and heat flow measurements, geochemical and petrological examination of Jurassic and Eocene magmatic rocks, and estimates of erosion rates from geomorphological data. We discuss and evaluate a set of possible mechanisms for lithospheric loss and intraplate volcanism beneath the region. Taken together, recent observations provide compelling evidence for lithospheric loss beneath the Central Appalachians; while they cannot uniquely identify the processes associated

with this loss, they narrow the range of plausible models, with important implications for our understanding of intraplate volcanism and the evolution of continental lithosphere. Our preferred models invoke a combination of (perhaps episodic) lithospheric loss via Rayleigh-Taylor instabilities and subsequent small-scale mantle flow in combination with shear-driven upwelling that maintains the region of thin lithosphere and causes partial melting in the asthenosphere.

Plain Language Summary

For the past 200 million years, the east coast of North America has been situated in the middle of a tectonic plate. Contrary to the expectations for this setting, a region of the Central Appalachian Mountains centered near the boundary between the U.S. states of Virginia and West Virginia exhibits atypical properties. The unusual observations include volcanic activity in the geologic past far away from a plate boundary, elevated rates of erosion associated with high topography in the Central Appalachians, and anomalous structure in the upper mantle that has been detected using geophysical methods. This paper describes, synthesizes, and compares a suite of observations that show that this part of the Central Appalachians is unusual compared to other so-called passive continental margins. We discuss a range of different models that might describe how the lithosphere, or the rigid part of the crust and upper mantle that defines the tectonic plate, has evolved through time beneath our study region. We show that the lithosphere today is thin, and that past episodes of lithospheric loss involving a portion of dense lithosphere “dripping” into the mantle under the force of gravity may provide a good explanation for the observations.

1. Introduction

Perhaps one of the most surprising and perplexing observations made over the past fifteen years of EarthScope and related science is the presence of an apparent "hole" in the lithosphere beneath the central Appalachians in Virginia and West Virginia that correlates very closely with the presence of comparatively recent (Late Jurassic and Eocene) volcanism. While the eastern margin of North America has undergone a series of major tectonic events over the past billion years of Earth history, these events significantly pre-date the volcanic episodes. The Grenville orogeny that took place at roughly 1 Ga culminated in the formation of the supercontinent Rodinia (e.g., McLelland et al., 2010; Whitmeyer & Karlstrom, 2007); Rodinia subsequently broke up between 750 and 550 Ma (e.g., Burton & Southworth, 2010; Li et al., 2008). The subsequent Appalachian orogenic cycle encompassed a protracted series of terrane accretion and mountain building events during the Paleozoic (e.g., Hatcher, 2010; Hibbard et al., 2010). The Pangea supercontinent was formed during the last phase of the Appalachian orogeny as Laurentia was joined to Gondwana. The breakup of Pangea, the final major tectonic event to affect the central Appalachians, began at roughly 230 Ma with rifting and extension, and the rift-to-drift transition was complete by approximately 185 Ma (e.g., Withjack et al., 1998; 2012). Rifting was accompanied by the emplacement of the Central Atlantic Magmatic Province (CAMP), one of the Earth's largest igneous provinces, over a period of less than one million years at approximately 200 Ma (e.g., Blackburn et al., 2013; Marzoli et al., 2018; McHone, 1996). Eastern North America thus assumed its current status as a passive continental margin by ~185 Ma, some 35 Ma before the first episode of anomalous central Appalachian volcanism.

The central Appalachians are not the only region to present evidence for passive margin lithospheric evolution. Across eastern North America, there are hints that, in some places,

112 modifications to lithospheric structure after the last major tectonic event (the breakup of Pangea
113 and the opening of the Atlantic Ocean basin) may have been profound. For example, there is
114 evidence for alkaline volcanism that post-dates CAMP in several regions along the margin (e.g.,
115 Mazza et al., 2017), including Jurassic kimberlitic magmatism in New York and Pennsylvania
116 (e.g., Bailey & Lupulescu, 2015; Bikerman et al., 1997), the Jurassic White Mountain Magma
117 Series and younger Cretaceous magmatism in New England (e.g., Foland et al., 1971; Kinney et
118 al., 2019), and the Cretaceous Monteregian Hills in eastern Canada (e.g., Foland et al., 1986).
119 Recent seismic imaging of upper mantle structure beneath eastern North America using data from
120 the EarthScope USArray Transportable Array (TA) has revealed evidence for complex upper
121 mantle structure (e.g., Biryol et al., 2016; Golos et al., 2018; Liu &Holt, 2015; Porter et al., 2016;
122 Schmandt & Lin, 2014; Wagner et al., 2018), including several prominent low velocity anomalies
123 that may hint at recent or ongoing dynamic processes. Furthermore, there is evidence from
124 geomorphological investigations for relatively recent rejuvenation of Appalachian topography
125 (e.g., Gallen et al., 2013; Miller et al., 2013; Pazzaglia & Brandon, 1996), perhaps reflecting
126 changes in dynamic topography generated by deep mantle flow (e.g., Rowley et al., 2013;
127 Spasojevic et al., 2008) and/or temporal changes in the density structure of the crust or mantle
128 lithosphere (e.g., Fischer, 2002; Wagner et al., 2012). Finally, there is ample seismicity along the
129 eastern North American margin (e.g., Wolin et al., 2013), much of it concentrated in zones that
130 may represent the reactivation of ancient structures in the present-day stress field (e.g., Thomas &
131 Powell, 2017).

132 Here we focus on the Central Appalachian Mountains, in a region encompassing the
133 boundary between Virginia and West Virginia (Figure 1). This region has hosted two pulses of
134 (spatially co-located) post-CAMP volcanism (at 152 Ma and 47 Ma; Mazza et al., 2014; 2017),

with the latter representing the youngest magmatic event in eastern North America. Taking advantage of newly available data from EarthScope and related projects, recent geophysical imaging has yielded evidence for anomalous structures in the crust and upper mantle beneath this region. This includes a prominent zone of low seismic velocities (e.g., Schmandt & Lin, 2014; Wagner et al., 2018), high seismic attenuation (Byrnes et al., 2019), and high electrical conductivity (Evans et al., 2019) in the upper mantle, with further evidence for thin mantle lithosphere from receiver function analysis (Evans et al., 2019). The seismic structure beneath the region is anomalous in several other ways, including a sharp lateral transition in crustal thickness (along a profile that is perpendicular to the strike of the Appalachian Mountains; Long et al., 2019) and an abrupt transition in SKS splitting behavior (Aragon et al., 2017).

The goal of this paper is to synthesize a suite of recent results from the Central Appalachian Mountains that have been enabled by EarthScope, GeoPRISMS, and related efforts in eastern North America. These include seismic and magnetotelluric imaging of the subsurface using data from the USArray Transportable and Flexible Arrays, geochemical and petrological investigations of post-CAMP magmatic products, geomorphological investigations of present-day erosion rates, and analysis of gravity and heat flow data. We include results from the MAGIC (Mid-Atlantic Geophysical Integrative Collaboration) experiment, which deployed a suite of densely spaced, co-located broadband seismic and magnetotelluric observatories across the Central Appalachians (Long et al., 2020). We discuss possible mechanisms for lithospheric loss and intraplate volcanism beneath the Central Appalachians and for the persistence of anomalous lithospheric structure over geologic time. These possible mechanisms include catastrophic lithospheric loss via Rayleigh-Taylor instability, gradual thermal erosion of the lithosphere, edge-driven convection, a deep mantle source of heat and/or hydration, shear-driven upwelling, or a combination of these. We

158 evaluate the strengths and weaknesses of different models and discuss how well each explains the
159 full range of observations. We present our preferred scenarios for lithospheric loss and intraplate
160 volcanism beneath the Central Appalachians, which invoke a combination of Rayleigh-Taylor
161 instability and shear-driven upwelling and/or small-scale mantle flow. Finally, we explore the
162 implications for a range of important outstanding Earth science questions and suggest avenues for
163 future progress on understanding the evolution of the Central Appalachians in particular and
164 continental lithosphere in general.
165
166 **2. Geophysical constraints**
167 *2.1 Seismic observations*
168 *2.1.1 Tomographic imaging of the Central Appalachian Anomaly*
169 Since the EarthScope TA traversed the eastern United States, a significant number of
170 papers have been published that image a volume of upper mantle with low seismic velocities that
171 has come to be known as the Central Appalachian Anomaly (CAA; e.g., Schmandt & Lin, 2014).
172 Data for these studies include Rayleigh waves from both ambient noise cross correlations (Bensen
173 et al., 2008; Golos et al., 2018; Pollitz & Mooney, 2016; Porter et al., 2016; Savage et al., 2017;
174 Schmandt & Lin, 2014; Schmandt et al., 2015; Shen & Ritzwoller, 2016; Wagner et al., 2018; Xie
175 et al., 2018) and teleseismic earthquakes (Babikoff & Dalton, 2019; Golos et al., 2018; Pollitz &
176 Mooney, 2016; Porter et al., 2016; Schaeffer & Lebedev, 2014; Schmandt et al., 2015; Shen &
177 Ritzwoller, 2016; Wagner et al., 2018; Yuan et al., 2014). Some studies have relied on teleseismic
178 body waves (Biryol et al., 2016; Golos et al., 2018; Savage, 2021; Schmandt & Lin, 2014; Wang
179 et al., 2019) and body waves from local seismicity (Wang et al., 2019).

The methodologies employed for determining spatial variations in velocity vary as well, particularly for those studies determining Rayleigh wave phase velocity maps that are subsequently inverted to create 3D shear wave velocity models. Several studies employed gradiometry (Lin et al., 2009) and/or Helmholtz (Lin & Ritzwoller, 2011) or Helmholtz-like (Pollitz & Snoke, 2010) wavefront modeling approaches that avoid the need for inversion and associated regularization (Babikoff & Dalton, 2019; Pollitz & Mooney, 2016; Porter et al., 2016; Schmandt et al., 2015; Shen & Ritzwoller, 2016) but that do depend on the grid spacing for the calculated derivates (Babikoff & Dalton, 2019). Of those studies that used inverse approaches, either for determining phase velocity maps or for body wave imaging, most used sensitivity kernels that incorporate finite frequency effects (Biryol et al., 2016; Golos et al., 2018; Savage et al., 2017; Schmandt & Lin, 2014; Wagner et al., 2018). Additionally, some studies used full waveform inversions of fundamental mode Rayleigh waves (Schaeffer & Lebedev, 2014; Yuan et al., 2014).

Despite the diversity of imaging approaches, most of these studies presented strikingly similar results in their identification of a small region of decreased seismic velocities in the uppermost mantle near the central WV/VA border. Figure 2 shows horizontal slices through the uppermost mantle (depth = 80 – 100 km) for a selection of six models that cover the CAA region (Boyce et al., 2019; Porter et al., 2016; Schmandt & Lin, 2014; Schmandt et al., 2015; Shen & Ritzwoller, 2016; Wagner et al., 2018). Three of these used a gradiometry/Helmholtz tomographic approach (Porter et al., 2016; Schmandt et al., 2015; Shen & Ritzwoller, 2016); Schmandt et al. (2015) and Shen & Ritzwoller (2016) added additional constraints from receiver functions and/or H/V ratios. Wagner et al. (2018) used a finite-frequency two-plane wave inversion for the determination of their phase velocity maps (Yang & Forsyth, 2006). Schmandt & Lin (2014) inverted teleseismic P and S-wave body waves with constraints from ambient noise phase

velocities to better define shallow structure. Boyce et al. (2019) performed an inversion of teleseismic P-wave body waves without any input from surface waves. All of these models show a very localized low-velocity region in the uppermost mantle, with lateral dimensions that are comparable to the interstation spacing of the TA and/or to the grid-node spacing employed in the inversion. This suggests that the anomaly may well be smaller than imaged, but it is unlikely to be much larger.

The surface wave-based models (Porter et al., 2016; Schmandt et al., 2015; Shen & Ritzwoller, 2016; Wagner et al., 2018) allow us to compare the absolute shear wave velocities observed within the uppermost mantle. Figure 3 shows cross-sections through all four models along transects roughly parallel to the MAGIC deployment. All of the seismic profiles show an abrupt decrease in seismic velocities (4.4 - 4.5 km/sec) for a relatively small region (< 150 km) along strike. This contrasts with the shear wave velocities observed at the same depth to the north and west which generally exceed 4.6 km/sec, consistent with relatively cold continental mantle lithosphere. Velocities also increase somewhat to the east of the CAA (between 4.5 - 4.6 km/sec), though these velocities are notably not as fast as those observed to the north and west (Vs > 4.6). Crustal velocities within the CAA are normal-to-slightly-elevated in the region above or near the low velocities in the uppermost mantle. There is no evidence in any model of reduced crustal seismic velocities associated with the CAA, as might be expected in the presence of a high geothermal gradient.

2.1.2 Seismic imaging across the dense MAGIC transect

The MAGIC seismic experiment (Long et al., 2020), part of the USArray Flexible Array, consisted of a linear deployment (roughly perpendicular to the strike of the Appalachian

Mountains) of 28 densely spaced broadband seismic stations across the CAA (Figure 1). The nominal station spacing was ~15 km in the region with anomalous post-CAMP volcanism and just under 30 km elsewhere. Estimates of depth to Moho across the MAGIC array derived from P-to-S receiver functions (Long et al., 2019) reveal evidence for a sharp "step" in the Moho just to the east of the Blue Ridge mountains (Figure 3; purple diamonds/line). This step involves a change in crustal thickness from roughly 48 km to the west to ~ 35 km to the east over a distance of ~15 km (Figure 3). The Moho step is located approximately 80 km to the east of the easternmost Eocene volcanic formation (Mole Hill, outside Harrisonburg, VA; see Figure 1). The step in the Moho does not appear to be a feature that is unique to the Central Appalachians; Li et al. (2020) argued that there is a Moho step near the western edge of Laurentian terranes throughout much of the central and northern Appalachians, extending north to roughly 43° latitude.

MAGIC data have also been used to document a sharp lateral transition in SKS splitting behavior across the Central Appalachian Mountains (Aragon et al., 2017). Figures 2 & 3 show SKS splitting measurements at stations of the MAGIC array; these exhibit a sharp transition from NE-SW fast directions at stations in the Appalachian Mountains to more E-W fast directions at stations located just to the east of the mountains. This transition in splitting behavior is roughly co-located with the easternmost occurrences of the post-CAMP igneous formations in the region. Aragon et al. (2017) suggested that SKS splitting reflects a combination of contributions from present-day mantle flow in the asthenosphere and lithospheric anisotropy frozen in from past tectonic processes. They further proposed that the lateral transition in splitting behavior is controlled mainly by the lithospheric component, although we explore an alternative explanation (one that invokes small-scale mantle flow) for this observation in this paper.

Constraints on present-day lithospheric thickness across the MAGIC array were obtained by Evans et al. (2019) through Sp receiver function imaging of the lithosphere-asthenosphere boundary (LAB). Their interpretations of the images suggest a lithospheric thickness of roughly 100-120 km beneath the eastern part of the MAGIC array. Directly beneath the Appalachian Mountains, Evans et al. (2019) identified a converter at ~80-90 km depth that dips gently to the west, likely corresponding to the LAB. Beneath the western half of the MAGIC array, a flat-lying converter at a depth of ~90 km likely corresponds to a mid-lithospheric discontinuity (MLD), while far to the west a prominent converter at a depth of ~140 km likely corresponds to the base of the lithosphere. Importantly, the Sp receiver function analysis of Evans et al. (2019) suggested thin (~80-90 km) lithosphere co-located with the tomographically imaged CAA.

Another result from the MAGIC experiment, based on seismic attenuation measurements, also suggests thin lithosphere beneath the Appalachian Mountains. Byrnes et al. (2019) modeled variations in the waveforms of first-arriving *P* phases from deep earthquakes recorded at MAGIC seismic stations using the approach of Bezada (2017) and Bezada et al. (2019). The result is a map of Δt^* values (Figure 2, grayscale; Figure 3, red line), a metric that is more positive when attenuation is stronger. Byrnes et al. (2019) observed low Δt^* values at the eastern and western ends of the MAGIC array, with much higher values (0.26 s) directly above the tomographically imaged CAA (Figures 2 & 3). For context, a 50 to 150 km change in lithospheric thickness, with *Vp* and *Qp* values taken from the lithosphere and asthenosphere in PREM (Dziewonski and Anderson, 1981), leads to Δt^* of only 0.03 to 0.09 s. Extrinsic attenuation due to either short- or long-wavelength variations in seismic velocity cannot explain the maximum in Δt^* at the CAA (Byrnes et al., 2019); rather, a thin lithosphere and particularly high attenuation in the asthenospheric upper mantle are required by the observations. Byrnes et al. (2019) suggested that

the values of *Qp* for the asthenospheric upper mantle beneath the CAA are low enough to require either partial melt (e.g., Abers et al., 2014) or a premelting effect that involves the disordering of grain boundaries as the solidus is approached (Yamauchi and Takei, 2016). More broadly, the attenuation results exclude the presence of either thick lithosphere or the replacement of lithosphere with "normal" sub-solidus asthenosphere in the CAA region.

MAGIC data were also used to investigate the detailed structure of the mantle transition zone beneath the Central Appalachians (Liu et al., 2018). Because the phase transformations associated with the 410 and 660 km mantle discontinuities are sensitive to temperature and water content, a detailed characterization of the transition zone can shed light on the thermal and hydration state of the mid-mantle and can reflect possible contributions from vertical mantle flow or from the presence of lithospheric fragments sinking through the mid-mantle (e.g., Benoit et al., 2013; Bina & Helffrich, 1994; Schmandt et al., 2012; Smyth & Frost, 2006). Images of the transition zone beneath the MAGIC array derived from single-station stacking of P wave receiver functions, migrated to depth using the iasp91 velocity model (Kennett and Engdahl, 1991), are shown in Figure 4. These images reveal that both the 410 and the 660 km discontinuities seem to deepen smoothly from west to east across the array, though the estimated thickness of the transition zone (which should be relatively insensitive to 3D velocity variations, which are not accounted for in our analysis) remains relatively constant. Previous work on transition zone structure beneath the southeastern U.S. using permanent seismic stations (Long et al., 2010) similarly suggested that transition zone thickness was generally uniform across the region and did not deviate significantly from standard mantle models. Keifer and Dueker (2019) applied Ps receiver function analysis to data throughout the central and eastern U.S. and found evidence for a region of anomalously thin (~230 km, as opposed to a nominal thickness of 250 km) transition zone beneath our study region.

However, they also found evidence for transition zone thinning beneath much of the eastern U.S., so this feature was not specific to the Central Appalachians. Work by Gao and Liu (2014) found little evidence for transition zone thinning beneath the eastern U.S. based on receiver functions; Wang and Pavlis (2016), who applied a 3-D wavefield imaging method, similarly found evidence for a generally standard transition zone thickness beneath our study region. The absence of significant variability in transition zone thickness across the MAGIC array suggests that there is likely little variation in the temperature or hydration state of the transition zone associated with the CAA anomaly. An alternative possibility is that any effects of lateral variations in temperature and hydration effectively balance each other out.

2.2 Electrical conductivity observations

Magnetotelluric data, collected as part of the MAGIC experiment (Long et al., 2020) and augmented by EarthScope TA coverage, highlight significant variations in lithospheric thickness across this portion of the central Appalachians (Evans et al., 2019). The electrical conductivity model of Evans et al. (2019), shown in Figure 3 (panel E), yields evidence for a variety of features, including thick lithosphere (>150 km) beneath the western part of the MAGIC profile and thin lithosphere (<75 km) directly along the CAA. In between the thick lithosphere to the NW and the thin lithosphere of the CAA lies a region of more conductive mantle at depths between ~100km-180km (100 – 400 km distance along the profile). Evans et al. (2019) interpreted this area as comprising lithospheric mantle affected by a combination of hydration and/or deformation (Pommier et al., 2018) that occurred during Grenville orogenic suturing. The conductivities of the CAA at depths greater than 80km are sufficiently high (> 0.1 S/m, corresponding to < 10 ohm-m) to require the presence of a small volume of partial melt (Evans et al., 2019). The inferences on

lithospheric thickness beneath the Appalachians gleaned from the electrical conductivity model are consistent with constraints from Sp receiver function analysis, and Evans et al. (2019) interpreted these datasets jointly.

2.3 Gravity and heat flow observations

In Figure 5A we show a map of Bouguer gravity anomaly from PACES (e.g., Stein et al., 2014) in a region surrounding the CAA. The well-known gravity low over the Appalachian topographic high and gravity high over the Piedmont are apparent in the Bouguer gravity plot (Pratt et al., 1988). The transition between the two is the Appalachian gravity gradient. Crustal thickening beneath the Appalachian Mountains has been proposed to explain the gravity low (Cook, 1984), while several explanations have been proposed for the gravity high. Interpretations have noted the correlations between the gravity high and the Carolina Slate (Long, 1979) or Mesozoic rift basins (Griscom, 1963), or attributed the gravity high to dipping structures imaged in seismic reflection data (Hutchinson et al., 1986) or subsurface loading (Karner & Watts, 1983). Following Stein et al. (2014), we upward continued the Bouguer anomaly data to 40 km and subtracted the result from the original Bouguer anomaly data, creating a "reduced" or upward continued Bouguer gravity map (Figure 5B). This procedure enhances anomalies from sources at greater depth and suppresses those from near surface sources (Jacobsen, 1987). We observed no striking correlation between the reduced Bouguer gravity map and the slow wavespeed anomaly documented in tomographic models (Figures 2 and 3) associated with the CAA, suggesting that there is no strong gravity anomaly associated with the other geophysical anomalies. The reduced Bouguer gravity map (Figure 5B) does show some hint of a gravity low in the CAA region, with a maximum amplitude of perhaps 35 mgal; however, there are similar gravity lows elsewhere along

strike in the central Appalachians, and there is no localized anomaly that matches the dimensions of the tomographically imaged CAA.

It is reasonable to question whether we would in fact expect to see a gravity anomaly due to a thermal anomaly in the uppermost mantle that has the dimensions of the tomographically imaged CAA. To illustrate the expected impact of a slow seismic anomaly on gravity, we assume that the anomaly is purely thermal. The temperature and density anomaly due to a thermal anomaly will be related by the coefficient of thermal expansion,

$$\delta\rho = -\rho\alpha\delta T \quad (1)$$

where ρ is the density, α is the coefficient of thermal expansion and T is the temperature, the minus sign indicates that a higher temperature results in a decrease in density. Using the solution for the gravity anomaly due to a buried sphere (Turcotte & Schubert, 2002) with a sphere of radius 50 km centered at 100 km depth, matching the peak 35 mgal gravity anomaly associated with the CAA requires a density contrast of -100 kg m^{-3}. This requires an unrealistically large temperature contrast of 1000^{o}C from Equation 1, with $\rho = 3300$ kg/m^3 and $\alpha = 3.0 \times 10^{-5\,o}$C^{-1}. A more realistic temperature contrast of 100-200^{o}C produces a Bouguer gravity anomaly of 3.5-7 mgals, which is small enough that it is unlikely to be observed. Using Birch's law (Birch, 1961),

$$v_p = -1.87 + 0.00305\rho, \quad (2)$$

where v_p is p wave velocity in km s^{-1} and ρ is density in kg m^{-3}, a 3% anomaly in v_p produces a 3% change in ρ. Hence, a 3% change in ρ is equivalent to -100 kg m^{-3}, assuming an upper mantle density of 3300 kg m^{-3}. While a direct comparison between a reasonable absolute v_p anomaly, as constrained by gravity data, and tomographic models (which constrain either absolute v_s or relative v_p values) is not straightforward, a 3% v_p anomaly is generally consistent with tomographic constraints.

This simple calculation, and the fact that we image a slow velocity anomaly of several percent beneath the CAA, but no large or prominent gravity anomaly that matches its dimensions, suggests that the anomaly is unlikely to be purely thermal; much of the velocity reduction may be due instead to the presence of partial melt and/or water. However, this inference would be complicated if there is also material with excess (positive) density in the crust or mantle lithosphere; in this case, the gravity signature from the less dense material (in the asthenospheric upper mantle) would destructively interfere with that from the more-dense material.

Inferences on the thermal state of the crust and lithosphere can in principle be gleaned from heat flow measurements and from the distribution of thermal springs in and around our study area; however, these indicators are difficult to interpret. The Virginia-West Virginia Hot Springs region (Bath and Highland Counties, Virginia and Pocahontas county, West Virginia, just to the south and west of the central part of the CAA) has the largest concentration of thermal springs in the eastern US, with more than 50 springs (Waring, 1965). Three prominent hot springs are shown in Figure 5. With the exception of one anomalously high heat flow value that is thought to be contaminated by groundwater circulation, heat flow in the Virginia-West Virginia Hot Springs region is consistent with the regional trend (Perry et al., 1979; Frone et al., 2015). As discussed by Evans et al. (2019), slightly elevated heat flow is observed across the Appalachians, with values between 70-80 mW/m^2 across the mountains (Frone et al., 2015). Overall, then, the evidence for locally high heat flow in the CAA region is mixed; while thermal springs are present, heat flow data do not show a pronounced anomaly in the vicinity of the CAA.

3. Petrological and geochemical constraints

The Central Appalachians have experienced two pulses of magmatism following the rifting of Pangea at 152 Ma and 47 Ma, co-located in a roughly 80 km by 50 km region that straddles the Virginia-West Virginia border (Johnson et al., 1971; Southworth et al., 1993; Mazza et al., 2014; 2017; Figure 1). The Late Jurassic magmatic event is characterized by a bimodal population of highly alkaline rocks, comprised of low silica basanites and high silica phonolites (Figure 6A). Mazza et al. (2017) explained the bimodal population as a result of fractional crystallization of the basanites at 10 kbar/35 km depth, near the base of an assumed 40 km thick crust. Calculated mafic melt equilibration temperatures from the Late Jurassic volcanics are consistent with normal asthenospheric mantle (~1350 °C, 2 GPa) and are too cold to invoke melting from a mantle plume (Mazza et al., 2017), but these calculations are limited to only one sample containing olivine. Radiogenic isotopes have been used as indicators for both assessing crustal interaction and differentiating mantle reservoirs. While Mazza et al. (2017) showed that the Late Jurassic event likely was unaffected by crustal assimilation, the geochemical and isotopic datasets for Central Appalachian crustal basement rocks are limited and do not include any of the mid-upper crustal carbonates that are abundant in the region. The Late Jurassic volcanics have a range of Pb radiogenic isotopes similar to volatile-rich lithologies such as carbonatites and kimberlites, with enrichment of radiogenic Pb coupled to magma evolution. Sr-Nd radiogenic isotopes are nearly identical to values reported from Late Jurassic kimberlites in New York (Figure 6C; Bailey & Lupulescu, 2015), which trend towards an enriched mantle component. The radiogenic isotope signatures from the Late Jurassic magmatic event in the Central Appalachians have been interpreted as melting of an enriched mantle source, mixing with an unsampled highly radiogenic Pb source that is potentially associated with metasomatism that is typical of kimberlite/carbonatite

409 magmas. Trace element signatures (Figure 6B) also imply the Late Jurassic basanites were
410 produced from low degree melting of an enriched asthenospheric source (~70 km depth).

411 The Eocene magmatic event is also characterized by bimodal, alkaline rocks, but these are
412 silica-saturated and are also characterized by lower abundance of alkaline elements than the Late
413 Jurassic event. The mafic population is comprised of picrobasalt to basalt magma containing Al-
414 augite and olivine phenocrysts, while the felsic population has an average trachydacite
415 composition (Figure 6A). Similar to the Late Jurassic event, the bimodal nature of the Eocene
416 event can be explained by fractional crystallization, with the felsic magmas forming at shallow
417 crustal depths of 2 kbar/7 km (Mazza et al., 2017). The Eocene mafic magmas are characterized
418 by typical ocean island basalt trace element signatures, suggesting they are the product of melting
419 an asthenospheric source (Figure 6B), in agreement with calculated mafic melt equilibration
420 temperatures and pressures consistent with normal asthenospheric mantle (~1400 °C and 2.3 GPa;
421 Mazza et al., 2014). The Eocene magmatic event was not affected by crustal contamination.
422 Instead, radiogenic isotopes from the Eocene volcanics suggest mixing between HIMU (high
423 $^{238}U/^{204}Pb$) and DMM (depleted mid-ocean ridge basalt mantle) mantle reservoirs, similar to many
424 of the Atlantic Ocean intraplate volcanoes (Mazza et al., 2014). The Eocene diatremes and some
425 of the dikes exhibit brecciated textures, carbonate inclusions within phenocrysts, and irregular
426 carbonate and zeolite amygdules within the volcanic groundmass (Haynes et al., 2014; Tso &
427 Surber, 2006), indicating the importance of volatiles in driving the Eocene eruptions. This is
428 consistent with high (>500 ppm) structural OH measured in clinopyroxene phenocrysts from
429 Highland County (Soles et al., 2014).

430 The structural features and petrography of the Eocene and Late Jurassic igneous bodies and
431 their xenoliths add to the regional context of the magmatism. Both pulses of magmatism were low

volume and exposed intrusive bodies vary from dikes ~10 cm in width to diatreme conduits ~200 m across. The Late Jurassic igneous rocks manifest as dikes that are preferentially oriented NW-SE, approximately perpendicular to the strike of regional folding (Southworth et al., 1993). The Eocene magmas produced dikes and diatreme structures (Haynes et al., 2014; Tso & Surber, 2006) that align with jointing and faulting within the host sedimentary units, predominantly trending to the NE-SW. The Eocene magmas are preferentially intruded into shale and carbonate units, though sandstone xenoliths within the basalts at Trimble Knob and Mole Hill indicate that some eruptions were able to punch through subsurface sandstone layers within duplex thrust splays or fold hinges (Johnson et al., 2013; Tso & Surber, 2006). Phenocrysts, xenocrysts, and xenoliths reveal information about the composition and temperature of the crust and lithospheric mantle. Clinopyroxene phenocrysts and xenocryst rims from the Eocene event record pressures corresponding to ~40 km depth, with temperatures ranging from 1230-1370°C (Johnson et al., 2013), which agrees with other calculations that indicate the Eocene event sampled the asthenospheric mantle. Paragneiss and syenite xenoliths are only confirmed to be found in Late Jurassic dikes. Paragneissic xenoliths experienced temperatures as high as 984°C from Zr-in-rutile thermometry and are of Grenville age, based upon detrital U-Pb zircon geochronology (Johnson et al., 2013).

The two post-rifting magmatic events that affected the Central Appalachians thus likely derived from the asthenospheric mantle at similar depths, but sampled geochemically distinct sources. The Late Jurassic event sampled a highly-enriched mantle domain that is similar to other magmatic events that effected the eastern margin of North America during the Late Jurassic (e.g. New York kimberlites), suggesting that this event might be associated with widespread magmatism. In addition, fractional crystallization of the more silica rich magmas occurred at the

455 base of the crust. On the other hand, the Eocene event shares geochemical and radiogenic isotopic
456 signatures of typical Atlantic intraplate volcanism with limited to no crustal interaction. The silica
457 rich magmas from the Eocene event evolved via fractional crystallization in the shallow crust.
458
459 **4. Geomorphological constraints**
460 Whether the present-day elevation and topographic relief along the Appalachian Mountains
461 represent continual, slow decay of remnant orogenic topography (e.g., Hack, 1960; Matmon et al.,
462 2003; Spotila et al., 2004) or reflect renewed rock uplift during the Cenozoic (e.g., Davis, 1889;
463 Pazzaglia & Brandon, 1996) remains a central question in the evolution of eastern North America.
464 Most workers agree that variations in the resistance of lithologic substrate to erosion along the
465 range manifest as differential landscape relief and rates of erosion (i.e., DiBiase et al., 2018; Hack,
466 1960; Hancock & Kirwan, 2007). However, variations in the pace of sediment delivery (Naeser et
467 al., 2016; Pazzaglia & Brandon, 1996), low-temperature thermochronology (Shorten and
468 Fitzgerald, 2020), the regional patterns of knickpoints preserved along some Appalachian river
469 networks (Gallen et al., 2013; Miller et al., 2013), and inverse models of stream profiles (Fernandes
470 et al., 2019) all imply that topographic relief increased during the late Cenozoic. Moreover, the
471 geodynamics driving such a change remain debated. For instance, in the Susquehanna River
472 watershed, north of our study area, regions of elevated channel steepness (a metric of channel
473 gradient normalized for basin drainage area; Wobus et al., 2006) and erosion rate were interpreted
474 to reflect an increase in river incision during the Neogene (Miller et al., 2013), perhaps reflecting
475 an increase in dynamic topography (Moucha et al., 2008; Moucha & Ruetenik, 2017; Rowley et
476 al., 2013). Similar patterns in topography and channel steepness in tributaries of the Tennessee
477 River, south of our study area, have been attributed to epierogeny (Gallen et al., 2013) but can also

478 be explained by river capture and drainage reorganization within approximately the same time
479 period (Gallen, 2018). These data were subsequently claimed to be consistent with dynamic
480 subsidence of the region driven by large-scale mantle flow (Liu, 2014). As our study area lies
481 between these two regions, the geomorphology of the range affords an opportunity to explore the
482 association between lithospheric architecture and potential changes in relief.

483 The high topography of the Appalachian Mountains above the CAA is characterized by
484 elevated channel steepness, relative to the Appalachians north and south, forming a broad
485 "bullseye" centered on the CAA, extending from southern West Virginia to the Pennsylvania
486 border (Figure 7A). Although the association of steeper channels with greater relief is not
487 surprising (e.g., DiBiase et al., 2010), elevated channel steepness indices along the crest of the
488 range are observed along both sides of the continental drainage divide (Figure 7D). This
489 observation suggests that elevated channel steepness is not simply a function of drainage capture
490 and divide migration (e.g., Naeser et al., 2016), but is characteristic of headwater regions of rivers
491 draining to both the Atlantic and Gulf of Mexico. Moreover, analysis of channel steepness as a
492 function of mapped lithology (see Supporting Information) reveals that channels are approximately
493 2-3 times steeper along the crest of the range, relative to its flanks, independent of substrate (Figure
494 7D). For instance, basins underlain by largely mudstone are present throughout a swath sampled
495 across the CAA (Figure 7D), and channels in these basins exhibit steepness indices of ~20-25 $m^{0.9}$
496 near the crest of the range, decreasing to values <5-10 $m^{0.9}$ east and west of the range. This
497 observation suggests that variations in channel steepness are not entirely a consequence of
498 variations in rock erodibility along the range.

499 To evaluate whether these spatial differences in channel steepness are in fact associated
500 with differences in erosion rate, we compiled previously published data on basin-wide average

erosion rates from studies of ^{10}Be concentrations in fluvial sediment from tributaries of the Potomac, James, and Susquehanna watersheds (Duxbury et al., 2015; Portenga & Bierman, 2011; Portenga et al., 2019). For each of these watersheds, we evaluated the network distribution of channel steepness (following methods of Harkins et al., 2007 and Perron & Royden, 2013) and substrate lithology from published regional geologic maps (Dicken et al., 2005; Nicholson et al., 2005). We focused our study on those 63 watersheds underlain by a single substrate lithology (Table S1). We compared channel steepness to erosion rate for each watershed (Figure S1); channel profiles that displayed significant convexities and knickpoints, considered to reflect potential transient, spatial variations in erosion rate (e.g., Kirby & Whipple, 2012), were eliminated from subsequent analysis. A detailed discussion of methods is available in the Supplemental Information. The remainder of the data define two distinct scaling trends between erosion rate and channel steepness (Figure 7B). Watersheds underlain by metabasalt and quartzite appear to be steeper, at a given erosion rate, than those underlain by metasedimentary and sedimentary rocks (Figure 7B). This analysis strongly implies that variations in channel steepness across the central Appalachians (background colors in Figure 7A) in the study area do, in fact, reflect variations in erosion rate. Steeper channels above the CAA appear to be eroding faster than the flanks of the range (Figure 7).

Overall, elevated rates of erosion along steep channels in the central Appalachians appear to be consistent with either: 1) maintenance of topography by ongoing differential rock uplift across the range, and/or 2) relatively slow decay of erosion rates from a past event that may have added buoyancy to the upper mantle and elevated the central Appalachians. Although our data are not sufficient to definitively discriminate between these scenarios, we can estimate the response timescales of a stream-power model of these fluvial networks (e.g., Goren et al., 2014). Although

524 such models are subject to significant limitations in how they represent the effects of stochastic
525 distributions of runoff and thresholds associated with bed sediment caliber (e.g., DiBiase &
526 Whipple, 2011; Lague, 2014), the linear scaling between channel steepness and erosion rate
527 presented here (Figure 7) suggests that stream-power type models capture at least the first-order
528 characteristics of the system. The linear scaling between channel steepness and erosion rate yields
529 a response time (τ) with the formula (Gallen, 2018; Goren et al., 2014)

530 $$\tau = \int_0^{x'} \frac{dx'}{K(x')A(x')^m} \quad (3)$$

531 where *x*' is the along-stream distance from the outlet, *K* is an erosion coefficient, *A* is upstream
532 drainage area, and *m* is a positive exponent related to the scaling of erosion rate with drainage area,
533 a proxy for discharge. To estimate the response time for the Potomac River basin, we used two
534 spatially-variable erosion coefficients, estimated as the inverse of the regressions (see Supporting
535 Information) relating channel steepness and erosion rate (Figure 7). We applied those coefficients
536 to other rock types not included in the erosion rate analysis because such data in those rock types
537 are absent (e.g., including carbonates in the more erodible, higher *K* class and igneous rocks and
538 remaining metamorphic rocks in the less erodible, lower *K* class). In this way, our analysis honors
539 the observation that the scaling of channel steepness depends on lithology (Figure 7D), although
540 it does not specify every rock type. The exponent *m* was set to 0.45, consistent with both theory
541 (Whipple & Tucker, 1999) and observation in the Susquehanna River basin (Miller et al., 2013).
542 For rivers of the approximate size of the Potomac, our analysis suggests that the response to a
543 simple perturbation in the relative rate of base level fall would sweep through the system within
544 20-30 Myr. Thus, while it is possible that elevated erosion rates and steep channels reflect
545 modifications of the lithosphere associated with the youngest phase of volcanism in Eocene time,

it seems unlikely that the geomorphology of this region of the Appalachians retains any signal of topographic changes that pre-date these events.

5. Synthesis of observations: An argument for lithospheric loss beneath the Central Appalachians

Taken together, the constraints from geophysics, petrology, geochemistry, and geomorphology described in Sections 2-4 form a suite of observations that suggest a past lithospheric loss event(s) and the preservation of a thinned continental lithosphere through geologic time. Our synthesis has documented a number of striking and anomalous observations associated with the CAA that any conceptual model for lithospheric evolution must be able to explain. To summarize, a number of geophysical imaging studies (Figures 2 and 3) have conclusively demonstrated that the lithosphere beneath the Central Appalachian Anomaly today is thin, with the LAB likely at ~75-90 km depth. These constraints include 1) tomographic imaging of low seismic velocities associated with the CAA, suggesting a region of absent lithosphere that is no wider than ~100 km and with low velocities extending to the base of the continental crust, 2) seismic attenuation measurements, which again suggest a region of thin lithosphere of limited lateral extent, 3) electrical conductivity measurements that require a shallow LAB and a highly conductive asthenosphere co-located with the tomographically imaged CAA, 4) Sp receiver function imaging, which suggests a shallow LAB that is spatially associated with the electrical conductivity anomaly, and is consistent with geochemically constrained asthenospheric melting depths.

The physical state of the upper mantle associated with the CAA today is therefore relatively clear – a thin lithospheric layer overlies an asthenosphere with geophysical indicators that are in

some ways more typical of mid-ocean ridge settings than ambient subcontinental asthenosphere. Resistivities below ~100 km depth are less than 10 Ωm (Evans et al., 2019), which is more conductive at comparable depths than beneath unmodified oceanic lithosphere (Sarafian et al., 2015) and comparable to asthenosphere beneath the East Pacific Rise at similar depths (Baba et al., 2006a,b; Key et al., 2013). The strength of attenuation is likewise comparable to that beneath the Juan de Fuca ridge (Eilon & Abers, 2017), or Lau (Wei & Wiens, 2018, 2020) and Marianas (Pozgay et al., 2009) back-arc spreading systems. Shear-wave velocities as constrained by surface waves are typically in the range of ~4.3-4.5 km/s at depths below 150 km beneath the CAA (Pollitz & Mooney, 2016; Porter et al., 2016; Shen & Ritzwoller, 2016; Wagner et al., 2018); these are more consistent with the asthenosphere beneath young oceanic plates than the continents (e.g., Lekic & Romanowicz, 2011). Taken together, the geophysical observations suggest the CAA comprises a region of partial melt at shallow depths below the continental crust over a very small (50 km radius) area.

The fact that these geophysical indicators of a region of absent mantle lithosphere and shallow partial melt are spatially co-located with the occurrence of Late Jurassic and Eocene volcanic and magmatic products (Figure 3) leads us to consider models that would explain both of these past episodes of tectonomagmatism and the present-day geophysical structure in terms of lithospheric loss and subsequent evolution. Key geochemical and petrological constraints that must be honored by such models include 1) the timing of the events, with one during the Late Jurassic and one during the Eocene, 2) the thermobarometry results, which suggest pressures (and thus depths) of melt equilibration of 2.1 GPa (roughly 70 km) for a Late Jurassic sample and 2.3 GPa (roughly 75 km) for Eocene samples, and temperatures that are associated with decompression melting of “normal” asthenosphere, and 3) the geochemical results, which for the Eocene event

592 similarly suggest decompression melting of “normal” asthenosphere from the sub-Atlantic Ocean
593 domain. Finally, the fact that the anomalous magmatic activity and present-day geophysical
594 anomalies are spatially co-located with relatively rapid erosion rates and steep channels also
595 pushes us to consider models for evolution of the Central Appalachian lithosphere that can explain
596 particularly rapid present-day erosion rates.

597 In other words, all available observations are consistent with shallow decompression
598 melting caused by lithospheric removal in the Jurassic, followed by a ~100 Ma hiatus (about which
599 we know very little), followed by another episode of small-scale volcanism during the Eocene
600 (which may or may not have included additional lithospheric removal), followed by some process
601 that has allowed for the maintenance of low seismic velocities, high seismic attenuation, low
602 resistivity, and high erosion rates for 47 million years. This means that we need to explain a) the
603 removal of mantle lithosphere on such a small scale, and b) the maintenance of such a small
604 lithospheric “hole” over geologic time.

605 In addition to the key geophysical, geomorphological, geochemical, and petrological
606 observations that suggest anomalous lithospheric evolution, we have also documented a number
607 of additional observations that may help to distinguish among different models. These include the
608 occurrence of a transition in SKS splitting behavior that is co-located with the CAA, the Moho
609 “step” that is just to the east of the Eocene volcanics, the observation of relatively “normal” and
610 unexciting transition zone structure beneath the CAA, the lack of pronounced anomalies in the
611 gravity and heat flow data, and the lack of a pronounced seismic velocity anomaly in the crust
612 above the upper mantle CAA.

613

614

6. Mechanisms for lithospheric loss and evolution beneath the Central Appalachians

Here we discuss and evaluate a range of possible conceptual models for a) lithospheric loss (and associated intraplate volcanism) beneath our Central Appalachians study area, and b) the evolution and maintenance of thin lithosphere over geologic time. Many of these ideas are based on previous work that have suggested mechanisms for explaining various observations (for example, low upper mantle seismic velocities, or the character and timing of volcanism). Section 6 focuses on a description of possible models, and Section 7 presents a comparison between predictions and observations. At this point, our evaluations of the various mechanisms are qualitative and conceptual; however, they represent a starting point towards more quantitative and specific comparisons between a working preferred model and observations, as described below.

6.1 Mechanisms for lithospheric loss

6.1.1 Localized loss via Rayleigh-Taylor instability

Mazza et al. (2014) proposed a localized lithospheric loss or delamination model for the central Appalachians as a mechanism to explain anomalous volcanism. This scenario invokes the gravity-driven loss of a small volume of lithosphere via a Rayleigh-Taylor instability (e.g., Elkins-Tanton, 2007; see sketch in Figure 8). We envision a localized (no more than ~100 km across, roughly the dimension of the present-day low velocity anomaly at depths of ~100 km) Rayleigh-Taylor instability of dense mantle lithosphere, perhaps also involving eclogitized, high-density lower crustal material. This lithospheric "drip" would have been relatively small in volume (with a diameter of ~100 km and a thickness of perhaps ~50-100 km, consistent with numerical modeling results; e.g., Conrad & Molnar, 1997), and after it detached and sank into the upper mantle, upwelling return flow would have resulted in decompression melting.

638

639 *6.1.2 Widespread lithospheric loss via Rayleigh-Taylor instability*

640 An alternative to the model of a localized gravity-driven lithospheric loss event is a
641 scenario in which a comparatively larger volume of lithospheric mantle was removed, with
642 subsequent thermal evolution (as discussed in section 6.2.1 below) that shrank the region of
643 thinned lithosphere to its present size. Such a scenario, to which the term "lithospheric
644 delamination" is often applied (e.g., Magni & Király, 2020), raises the possibility that a
645 substantially larger portion of the mantle lithosphere was initially lost than envisioned in section
646 6.1.1 above. Our motivation for considering this idea is that in this scenario there is no need to
647 invoke a set of processes that maintain the configuration of the lithosphere that was created by the
648 most recent lithospheric loss event over long periods of geologic time. Instead, we envision that
649 after the lithospheric loss event, the lithosphere progressively cooled and thickened; in the course
650 of this evolution, what was initially a larger lithospheric "divot" shrank to its present dimensions.

651

652 *6.1.3 Gradual thinning of the lithosphere via thermal ablation*

653 Evans et al. (2019) suggested a model of gradual, rather than a catastrophic, lithospheric
654 loss beneath the Central Appalachians as a possible alternative to gravity-driven instability. We
655 envision a scenario in which some initial perturbation of the "topography" at the base of the
656 lithosphere, perhaps tied to preexisting or inherited lithospheric structure from earlier processes,
657 allowed for the localization of upwelling mantle flow and the progressive thermal ablation or
658 erosion of the lithosphere to its present-day configuration. Evans et al. (2019) invoked the idea of
659 shear-induced upwelling as a possible mechanism for this process; if variable topography on the
660 lithosphere, and/or lateral variations in mantle viscosity, led to shear-driven upwelling (e.g.,

661 Ballmer et al., 2015; Conrad et al., 2010, 2011), then any melt produced would migrate to the
662 shallowest point of the LAB. Melt ponded at the LAB may then play a role in thermally eroding
663 the lithosphere via dike intrusion (e.g., Havlin et al., 2013); this model predicts that over time, the
664 lithosphere progressively erodes and evolves to its present-day configuration. This model does
665 not make specific predictions about the time frame of the gradual lithospheric thinning, and the
666 timescale over which this may have occurred is not well constrained. Havlin et al. (2013) suggested
667 that this type of mechanism, with modest melt fractions, can thin the lithosphere by roughly 50 km
668 or more over a 50 Myr time frame.
669
670 *6.1.4 Lithospheric thinning via edge-driven convection*
671 Another possibility is that the present-day low velocities beneath the Central Appalachians
672 represent the upwelling limb of a small-scale convection cell that is driven by downwelling at the
673 edge of the thick portion of North American cratonic lithosphere to the west. This model invokes
674 the classic edge-driven convection scenario of King and Anderson (1998) and King (2007), which
675 has been considered before in a slightly different context as an explanation for processes occurring
676 beneath the southeastern U.S. (Benoit et al., 2013; Long et al., 2010). The concept of edge-driven
677 convection has been applied to explain lithospheric thinning and intraplate volcanism in other
678 geographic settings (e.g., Kaislaniemi & van Hunen, 2014; Van Wijk et al., 2010), and has also
679 been invoked to explain the Northern Appalachian Anomaly, another low-velocity upper mantle
680 anomaly associated with thinned lithosphere that is centered under New England (e.g., Dong &
681 Menke, 2017; Levin et al., 2018; Menke et al., 2016, 2018). In this model, the upwelling limb of
682 the convection cell causes decompression melting and corresponds to the present-day low velocity
683 anomaly in the upper mantle; the upwelling may have contributed to lithospheric thinning over

684 time through thermal ablation, yielding the thin lithosphere that is inferred today. While this model
685 is not temporally specific in the same way that the catastrophic lithospheric loss is, the edge-driven
686 convection cell may have been present continuously (or at least episodically) for long periods of
687 geologic time if it is to be invoked as an explanation for past intraplate volcanism in our study
688 region.
689
690 *6.1.5 Lithospheric thinning driven by a deep, plume-like upwelling*
691 Yet another plausible scenario invokes deep processes, rather than processes taking place
692 in the upper mantle, as the driver for melting and volcanism beneath the Central Appalachians.
693 This model invokes the presence of an anomaly in the mid-mantle (or deeper) as the trigger for
694 melting and as the explanation for the present-day low velocity zone and thin lithosphere. This
695 anomaly could take the form of a classical thermal mantle plume, which may have been able to
696 thermally ablate or thin the lithosphere when it passed through. Alternatively, it could take the
697 form of a "wet spot" whose increased water content lowers the melting temperature and enables
698 melting, and may contribute directly to the reduced seismic velocities in the upper mantle. Each
699 of these two scenarios has been previously proposed in the literature. Chu et al. (2013) proposed
700 the presence of a "hidden hotspot track" beneath the central and Eastern U.S. on the basis of
701 seismic waveform modeling that suggested two corridors of modified lower lithosphere with
702 reduced seismic velocities and enhanced seismic attenuation. Van der Lee et al. (2008) previously
703 suggested pervasive hydration of the upper mantle beneath eastern North America on the basis of
704 documented low-velocity anomalies beneath the Eastern Seaboard in tomographic models that
705 predate the deployment of the EarthScope USArray (e.g., Van der Lee & Frederiksen, 2005). In
706 the Van der Lee et al. (2008) model, hydration and upwelling were invoked to explain a broad

region of lower than average upper mantle velocities beneath the eastern U.S.; in contrast, here we invoke the possibility of a much narrower and more localized hydrous upwelling as a source of melt production directly beneath the Central Appalachians.

6.2 Scenarios for evolution of thinned lithosphere over time

We envision several possible scenarios for how the lithosphere may have evolved after a lithospheric loss event by any of the mechanisms discussed in section 6.1. These models may include gradual thermal healing of thinned lithosphere (perhaps accompanied by temporal changes in density structure) or mechanisms that can maintain a thin lithosphere over time, including shear-driven upwelling or continuous or episodic edge-driven convection.

6.2.1 Gradual thermal healing of thinned lithosphere

The simplest and most straightforward idea for the temporal evolution of the lithosphere after an episode of lithospheric loss or removal is the gradual healing or re-forming of the lithospheric mantle through time. While a lithospheric loss event would likely be accompanied by upwelling and perhaps heating of the base of the of the lithosphere, over time one might expect the continental lithosphere to thicken and densify as it progressively cools, much as oceanic lithosphere evolves as it ages and moves away from the mid-oceanic ridge. In addition to the increase in density expected as the lithosphere cools, changes in its density structure due to metamorphic reactions (e.g., Fischer, 2002) are also possible. We would generally expect that a mechanism of thermal healing would slowly thicken the lithosphere over time, causing an initial "hole" or "divot" to gradually disappear through progressive thickening.

730 *6.2.2 Maintenance of thinned lithosphere via small-scale mantle flow and shear-driven upwelling*

731 If one or more lithospheric loss events took place beneath the central Appalachians in the
732 geologic past, then a potential mechanism is needed to maintain the thinned lithosphere over
733 geologic time (rather than allowing for thermal healing via the slow regrowth of lithosphere
734 through gradual cooling). Small-scale mantle flow driven by the motion of the North American
735 Plate may have played a role in maintaining the "hole" or "divot" in the lithosphere. One possibility
736 is that as the plate continued to move over the asthenospheric mantle beneath it, it induced a small-
737 scale mantle flow cell within the divot itself (see Figure 8), continuously bringing relatively hot
738 asthenospheric upper mantle into contact with the base of the lithosphere and preventing thermal
739 healing of the lithospheric divot. This idea is similar to the concept of shear-driven upwelling as a
740 mechanism to produce melting and volcanism in intraplate settings (Conrad et al., 2010, 2011).
741
742 *6.2.3 Maintenance of thinned lithosphere via continuous or episodic edge-driven convection*

743 As discussed in section 6.1.4, edge-driven convection has been suggested as a possible
744 mechanism to explain volcanism in the Central Appalachians and in other intraplate settings. Edge-
745 driven convection may be more or less continuous, with nearly continuous downwellings initiated
746 at the base of the thick continental lithosphere near its edge, or it may be episodic, with an abrupt
747 episode of downwelling (accompanied by upwelling return flow on the other limb of the
748 convection cell) followed by a period of quiescence and ultimately another pulse of mantle flow
749 (perhaps associated with an abrupt change in plate motion). If edge-driven convection is present
750 beneath the Central Appalachians, then it may have played a role in maintaining a relatively thin
751 lithosphere over long periods of time through multiple episodes of downwelling, upwelling return

752 flow, and lithospheric thinning, or through a continuous (or nearly continuous) version of this
753 process.
754
755 **7. Which models are most consistent with the observations?**
756 *7.1 Mechanisms for lithospheric loss and evolution: Comparison with observations*
757 *7.1.1 Lithospheric loss via localized gravity-driven instability*
758 Lithospheric loss via a relatively small gravity-driven Rayleigh-Taylor instability during
759 the Eocene (and perhaps also during the Jurassic, if the loss was episodic) is generally consistent
760 with many of the observations. Specifically, this mechanism is compatible with the primitive
761 composition and estimated depths and temperatures of melt equilibration of the Eocene magmatic
762 products, as argued by Mazza et al. (2014). It is also consistent with the observations of the present-
763 day upper mantle anomalies in seismic velocities, seismic attenuation, and electrical conductivity
764 (Figure 3). All of these indicators, along with the Sp receiver function imaging, are consistent with
765 thin lithosphere beneath the Central Appalachians, directly beneath the Eocene volcanic and
766 magmatic products at the surface. This mechanism can explain the small size and the spatial
767 location of the upper mantle anomalies, in that the present-day lithosphere is thin in the region
768 where a small volume of lithosphere was presumably lost during the Eocene.
769 If a small volume of lithosphere were removed via gravitational instability during the
770 Eocene, then we might consider whether we might expect to image a lithospheric fragment in the
771 mantle transition zone. Given its small dimensions (~50 km radius), any detached lithosphere
772 should have thermally equilibrated with the surrounding asthenospheric mantle fairly quickly as it
773 sank. Specifically, the timescale for heat to diffuse over a distance, d, is given by
774 $$t_d \sim \frac{d^2}{4\kappa} \quad (4)$$

where κ is the thermal diffusivity, which for the mantle is ~10^{-6} m^2 s^{-1}. A sphere of lithosphere with 50 km radius would thus thermally equilibrate with the surrounding asthenospheric mantle on the order of 20 Myr. The observed lack of strong topography on the mantle transition zone discontinuities beneath the Central Appalachians (Figure 4) can therefore be considered as consistent with lithospheric loss via Rayleigh-Taylor instability during the Eocene (and/or earlier).

The length and time scales of lithospheric Rayleigh-Taylor type instabilities have been estimated by Conrad & Molnar (1997). Including the effect of thermal diffusion, instabilities grow most rapidly at wavelengths on the order of 100-200 km. Assuming an asthenospheric viscosity of 10^{19} Pa s, the instabilities grow by a factor of *e* every 3-5 Myr. Because such instabilities only displace the bottom one third to one half of the lithosphere (e.g., Conrad & Molnar, 1997), these instabilities would produce only small anomalies in topography and gravity at the Earth's surface above the downwelling, consistent with the (lack of) observations.

The region of inferred lithospheric loss is just to the west of the sharp step in the Moho, but possible links between them remain unclear. The particularly thick crust (~50-55 km; Long et al., 2019) beneath the Central Appalachian Mountains (Figure 3) may point to the presence of unusually dense, perhaps eclogitized, material in the lower crust today. There is some additional support for the idea of particularly dense lower crust, at least during the Late Jurassic, from the observation of xenoliths of garnet-rich gneisses in the lower crust, found in Late Jurassic magmas (Johnson et al., 2013). It is unclear, however, whether such material may have been present in the geologic past and whether it may have played a role in triggering the Rayleigh-Taylor instability through which the lithosphere was lost. If eclogitized lower crustal material was involved in the episode of lithospheric loss during the Eocene, then that might suggest that the crust beneath the mountains was even thicker in the geologic past.

798 It is not clear whether the observed elevated rates of present-day erosion in the Central
799 Appalachians (Figure 7) might be directly associated with an episode of lithospheric removal
800 during the Eocene. If a Rayleigh-Taylor instability removed a portion of dense lithosphere and
801 therefore adjusted the overall buoyancy of the system during the Eocene, then uplift and enhanced
802 erosion would be expected. It is unclear, however, whether the present-day erosion rates would be
803 expected to still reflect this event, given the timescales involved. As discussed in section 4, simple
804 scaling arguments suggest that the timescales of response for the rivers draining the Central
805 Appalachians today are no greater than ~30 Ma. Unless any pulse of enhanced uplift and erosion
806 has decayed more slowly than expected (c.f. Baldwin et al., 2003), it is difficult to directly link
807 elevated present-day erosion rates with an episode of lithospheric loss during the Eocene. An
808 indirect link may be possible, however, if the lithospheric divot is being maintained via small-scale
809 mantle flow today, as discussed further in 7.1.6 below.
810 While Mazza et al. (2014) proposed a lithospheric loss scenario to explain Eocene
811 volcanism, it is possible that there were in fact multiple episodes of catastrophic lithospheric loss
812 beneath the region, perhaps corresponding to both the Jurassic and Eocene volcanic pulses. One
813 possibility is that some aspect of lithospheric structure beneath the Central Appalachians has made
814 it particularly prone to gravitational instability – perhaps related to lithospheric weakening, or to
815 its density structure – that may have been created or "seeded" during the breakup of Pangea. A
816 possible scenario is that a Rayleigh-Taylor instability led to the loss of lithosphere in the Late
817 Jurassic, causing upwelling return flow and decompression melting, and leading to magmatic
818 activity at the surface (Mazza et al., 2017). This event may well have modified the structure of the
819 crust and/or remaining lithospheric mantle, and may have emplaced particularly dense material
820 (i.e., underplated mafic rocks) at the base of the crust, perhaps priming the system for another,

821 later phase of lithospheric loss. Between the Late Jurassic and the Eocene, the structure of the
822 lithosphere may have evolved and been modified via thermal healing; furthermore, the density
823 structure of the deep crust may have evolved, perhaps through time-progressive metamorphic
824 reactions (e.g., Fischer, 2002; Williams et al., 2014). As the system evolved through time, the
825 lithosphere beneath the Central Appalachians may have become more gravitationally unstable,
826 perhaps via a combination of the changing density structure (as the lithosphere cooled) and through
827 preexisting factors such as the presence of low-viscosity lithosphere (either from the tectonic
828 inheritance of preexisting weak zones, the presence of volatiles such as water, or other factors).
829 This may have led to a second lithospheric loss event during the Eocene, which led to a similar
830 scenario of upwelling return flow, the production of partial melt, and the transport of that melt
831 through the overlying crust to the surface.
832
833 *7.1.2 Gradual lithospheric thinning via thermal ablation*
834 A gradual lithospheric thinning mechanism could also be considered as generally
835 consistent with the imaging of the present-day lithospheric structure beneath the Central
836 Appalachians. Such a mechanism can explain the size and location of the upper mantle anomalies
837 in seismic velocity, attenuation, and electrical conductivity; in particular, this model, which
838 appeals to the ponding of melt at the shallowest point of the lithosphere as it gradually thins, is
839 consistent with the inference from both electrical conductivity and attenuation measurements that
840 partial melt may be present in the shallow asthenosphere today. Furthermore, this mechanism may
841 provide a natural explanation for the persistence of the lithospheric divot over geologic time
842 (without needing to appeal to a process such as edge-driven convection to maintain it).

On the other hand, a mechanism that invokes gradual thinning cannot explain the temporal specificity of the Late Jurassic or Eocene volcanism. In the context of this mechanism, additional processes (such as the reactivation of crustal structures and/or the reorganization of the crustal stress field) must be invoked to explain the timing of pulses of volcanic activity. Interestingly, the bend in the Hawaii-Emperor seamount change suggests a global reorganization of plate motions at roughly ~47 Ma (e.g., Wright et al., 2015); while this is speculative, in the context of this model this global change may have reorganized the stress field in our study region and allowed for the migration of melt to the surface (e.g., Southworth et al., 1993). This would mean that the lithospheric geometry seen today may have been established in the Jurassic (producing the initial episode of magmatism) and may have changed little since that time. In this framework, the Eocene volcanism only occurred due to a passing favorable re-organization of stresses and associated opening of crustal magmatic conduits, or due to a transient episode of more intense upwelling and melt production associated with a change in plate motion. (It is worth noting that this idea may apply regardless of the mechanism for lithospheric removal during the Jurassic, whether it was catastrophic or gradual.)

Gradual thinning of the lithosphere would predict that the equilibration depths of mantle-derived melts should decrease over time; however, this prediction is not particularly well borne out by petrological observations. Specifically, Mazza et al. (2017) found an equilibration pressure of 2.09 GPa (roughly 70 km) for a Late Jurassic sample (Sample #31), compared with equilibration pressures of 2.32 ± 0.31 GPa for Eocene samples (Mazza et al., 2014). We note, however, that direct comparisons are difficult, because data for the Late Jurassic are limited; most of the Late Jurassic samples are highly alkaline, precluding the use of traditional geothermobarometers due to the mineralogy and magma composition (Mazza et al., 2017).

866

867 *7.1.3 Widespread lithospheric loss with subsequent healing/regrowth*

868 A mechanism of widespread lithospheric loss (that is, a Rayleigh-Taylor instability whose
869 dimensions were significantly larger than the present-day upper mantle geophysical anomaly)
870 could be generally consistent with the timing and petrological characteristics of Central
871 Appalachian volcanism, but not their spatial localization. Specifically, if a large volume of
872 lithosphere had been removed, then volcanism over a wider region would be expected; instead, the
873 expression of Eocene magmatism at the surface is localized to a small region of western Virginia
874 and eastern West Virginia (Figure 1). This mechanism also does not provide a particularly specific
875 explanation for the location of the present-day upper mantle velocity, attenuation, and conductivity
876 anomalies, or for their co-location with the Eocene volcanics. We can conjecture that the present-
877 day location of the CAA corresponds to the center of the region of lithospheric loss (that is, where
878 the thickest column of lithosphere was removed), but this is speculative. This model is generally
879 difficult to reconcile with constraints provided by modeling studies of Rayleigh-Taylor instabilities
880 (e.g., Conrad & Molnar, 1997), which suggest that long-wavelength instabilities would create
881 surface deformation; evidence for this is not observed. Furthermore, if a large amount of material
882 was removed during a past episode(s) of lithospheric loss, we might expect to be able to observe
883 it as a high-velocity anomaly in the mantle today (for a spherical anomaly with a radius of ~500
884 km, the thermal diffusion time would be roughly 2 Gyr), and we do not.

885 One aspect of the observations that could potentially be explained by this mechanism is the
886 inference of altered mantle lithosphere just to the west of the upper mantle conductivity anomaly,
887 as discussed by Evans et al. (2019). They hypothesized that the mantle lithosphere here has
888 undergone alteration due to deformation via shearing or through hydration, leading to higher

conductivity values than is expected for typical continental mantle lithosphere (such as those observed further to the west along the MAGIC profile). It is possible that these alteration processes may reflect the evolution of the mantle lithosphere through healing and thermal regrowth, if this portion of the lithosphere was included in a hypothetical larger lithospheric loss event. However, lithosphere would generally be expected to thermally heal from the top down, rather than laterally, making it somewhat difficult to envision how an initially large area of thinned lithosphere might shrink in lateral extent (that is, in map view) while maintaining a shallow LAB. It is thus difficult to envision a physically reasonable mechanism for the evolution of a past large lithospheric divot or hole to the configuration that we image today.

7.1.4 Edge-driven convection

An edge-driven convection mechanism for lithospheric thinning (and/or the maintenance of thin lithosphere through geologic time) fails to match the observations beneath the Central Appalachians in several key aspects. This model does not easily explain the temporal specificity of the Late Jurassic or Eocene magmatic activity, unless episodic edge-driven convection is invoked, and even then, it is not easy to reconcile the persistence of the geophysical anomalies into the present day unless other processes are involved. Edge-driven convection is also not easily reconciled with the spatial localization of both the magmatic pulses and the present-day geophysical anomalies in the upper mantle; if small-scale convection driven by downwellings at the edge of the thick North American cratonic lithosphere to the west is driving upwelling and volcanism beneath the Central Appalachians, then why do we not observe intraplate volcanism and upper mantle anomalies everywhere along the margin? (One possibility, of course, is that the vigor and/or periodicity of edge-driven convection may vary along strike; previous work (e.g., Till

et al., 2010) has shown that the size of the edge-associated downwelling depends on the sharpness of the edge, so along-strike variability in edge-driven convection could reflect along-strike differences in lithospheric architecture.)

If edge-driven convection were active today beneath the Central Appalachians, we would expect upwelling in the upper mantle beneath our study area; the vertical shearing produced by such an upwelling should produce vertically oriented fast axes of seismic anisotropy and would therefore predict negligible shear wave splitting stemming from anisotropy in the asthenospheric upper mantle. This is not obviously consistent with the SKS splitting observations in our study region (Figure 3), which exhibit a modest rotation in fast splitting directions near the Central Appalachian Anomaly but no significant local minimum in splitting delay times. Of course, this prediction could be complicated by the presence of anisotropy in the mantle lithosphere; however, the thin (~80 km) lithosphere that is present beneath the Central Appalachians implies that a significant contribution to SKS splitting from the asthenospheric upper mantle is likely (Aragon et al., 2017). We further acknowledge that flow patterns in the mantle are likely to be complex and even in areas of upwelling, the regions of null SKS splitting may be spatially restricted (e.g., Blackman & Kendall, 2002), so comparisons between SKS splitting and predictions for edge-driven convection models are not straightforward.

The predictions that the edge-driven convection model would make about transition zone structure are a bit ambiguous. If an edge-driven convection cell exists today and is confined to the upper mantle, then we would expect no effect on the mantle transition zone discontinuities. However, if a present-day convection cell is larger and the mantle flow associated with it penetrates the mantle transition zone, then we might expect to see a localized thinning of the transition zone beneath the Central Appalachians. Data from the MAGIC array indicate no such localized thinning

(Figure 4), and studies based on USArray TA data mostly argued against transition zone thinning beneath our study region (Liu & Gao, 2014; Wang & Pavlis, 2016), although Keifer and Dueker (2019) did find some evidence for a thin transition zone beneath the Central Appalachians.

7.1.5 A deep thermal or hydrous mantle anomaly

A mechanism for lithospheric thinning that invokes a deep source of heat (via a thermal mantle plume) and/or hydration makes some specific predictions about mantle structure that are, for the most part, not borne out by the observations. There is little or no evidence for a deep mantle plume, or for a localized conduit of particularly hydrated mantle that is connected to a source in the deep mantle, in images of present-day mantle structure. While the Central Appalachian upper mantle velocity anomaly is a robust feature in most tomography models (Figures 2 and 3), there is little or no evidence that it is connected to slow structures in the transition zone or lower mantle (e.g., Biryol et al., 2016).

A model of a thermal or hydrous plume conduit that is fed by the deep mantle and remains stationary in a mantle reference frame while the North American plate moves above it is also difficult to reconcile simultaneously with presence of geophysical anomalies in the shallow upper mantle today and with magmatic activity during the Late Jurassic and Eocene. While a mantle plume has been proposed as a possible explanation for intraplate volcanism in eastern North America, including the Eocene volcanics (Chu et al., 2013), the motion of the North American plate (absolute plate speed of ~34 mm/yr relative to the mantle beneath, in the hotspot reference frame of the HS3-Nuvel 1A model; Gripp & Gordon, 2002) means that the present-day location of the mantle plume would be roughly 1600 km to the east, and the upper mantle geophysical anomalies would not be particularly well explained. Conversely, if the plume were located beneath

the Central Appalachians today, then it could be invoked as an explanation for the geophysical anomalies but would not be a good explanation for the intraplate volcanism. The co-location of the Eocene and Late Jurassic magmatic products with the present-day geophysical anomalies is thus not easy to reconcile with the concept of a deep mantle source, unless one assumes that the upper mantle geophysical anomalies were caused by the passage of a mantle plume in the past and then have been maintained over time through other processes.

As with the edge-driven convection mechanism, a plume model would predict upwelling flow in the upper mantle (if the plume were located beneath the Central Appalachians today), which is not particularly consistent with the SKS splitting observations (Figure 3), although SKS splitting patterns predicted by plume models are often complex and depend on a number of factors (e.g., Ito et al., 2015). A model that invokes a hot or hydrous upwelling from the deep mantle would also predict complexities in transition zone structure, including transition zone thinning (via the depression of the 410 km discontinuity and the elevation of the 660 km discontinuity; e.g., Bina & Helffrich, 1994) if thermal effects dominate. As discussed by Long et al. (2010), a hydrous transition zone such as that proposed by Van der Lee et al. (2008) would predict a shallowing of the 410 km discontinuity of ~20-40 km under water-saturated conditions (Smyth & Frost, 2002), producing ~20-40 km of transition zone thickening. Neither of these effects is observed; the transition zone thickness beneath the MAGIC line (Figure 4) is close to the global average.

7.1.6 Maintenance of thin lithosphere via shear-driven upwelling

The idea that the lithospheric divot that is observed today results from one or more past episodes of catastrophic (but relatively localized) lithospheric loss and has been maintained by small-scale mantle flow and shear-driven upwelling due to the motion of the North American Plate

over the mantle beneath it makes a few predictions that can be tested with our observations. This mechanism is generally consistent with the inference that there may be partial melt in the uppermost mantle beneath the CAA today, as suggested by Evans et al. (2019) and Byrnes et al. (2019), as ongoing shear-driven upwelling would result in a continuous process of decompression melting. It may also be consistent with SKS splitting observations, in that it may provide an explanation for the rotation in SKS fast splitting directions observed in western Virginia (Figure 3). Specifically, if the overall upper mantle flow field (likely dominated by plate-motion-parallel shearing; e.g., Long et al., 2016; Yang et al., 2017) is being locally disturbed by small-scale flow associated with shear-driven upwelling, then this may explain the local change in SKS splitting behavior. While we do not observe the weak or absent SKS splitting that would be predicted for truly vertical shearing over a substantial area (e.g., Levin et al., 2018; Long et al., 2010), the scale of a possible shear-driven upwelling is likely small enough that we would not predict a clear transition to null or absent splitting in the SKS data. (We caution that there are other ways to explain the lateral variation in SKS splitting behavior, as it may plausibly be dominated by contributions from frozen-in structure in the lithosphere, rather than present-day mantle flow.)

The notion of small-scale mantle flow that includes an upwelling component is also generally consistent with the observation of elevated erosion rates along steeper channels in the Central Appalachians today (Figure 7). The present-day scaling of erosion rate, channel steepness and erosional efficiency for these rivers suggest a response timescale of ~30 Ma, which is less than the time elapsed since the last episode of volcanism during the Eocene. If the elevated rates of erosion instead reflect ongoing uplift or buoyancy from the upper mantle, then this would be broadly consistent with ongoing shear-driven upwelling associated with small-scale mantle flow within the lithospheric divot (Figure 8).

One aspect of the present-day geophysical structure that is not explained well by a shear-driven upwelling mechanism to maintain the lithospheric divot is the velocity structure of the crust above the CAA (Figure 3). Specifically, the lack of a crustal low-velocity anomaly is puzzling, as one would expect the crust overlying the thinned lithospheric mantle to undergo warming over geologic time and to display lower velocities today if shear-driven upwelling of the asthenosphere has been continuously operating since at least the Eocene. Of course, if there was a compositional effect on crustal velocities in the region, with anomalously fast velocities due to compositional variations, then this effect could in theory offset a potential thermal effect.

7.2 Preferred models for lithospheric evolution beneath the Central Appalachians

The comparisons between observations and the predictions of various mechanisms of thinning the lithosphere and maintaining thin lithosphere through time described in Section 7.1 lead us to a small set of preferred models for the evolution of the Central Appalachian lithosphere since the breakup of Pangea. We emphasize that our preferred models are not perfect and are not completely consistent with the full range of observations. Furthermore, at this point our comparisons between model predictions and observations is almost entirely qualitative, and more specific, detailed, and quantitative modeling is needed in the future to link model predictions more definitively to observations. Despite these limitations, however, we can present a small set of favored models that are better able to match the observational constraints than others.

Given the preponderance of the observational evidence, we see the scenarios illustrated in Figure 8 as being most consistent with the full range of available constraints. We suggest that there was an episode of lithospheric loss during the Late Jurassic, perhaps via a gravitationally driven Rayleigh-Taylor instability that removed a relatively small volume of lithosphere, or perhaps due

1027 to another process such as thermal ablation. This lithospheric loss event was associated with
1028 upwelling return flow triggering decompression melting and magmatic activity at the surface.
1029 After this Late Jurassic episode, we envision two possibilities to explain the Eocene volcanics. The
1030 first is that there was a second episode of lithospheric instability and loss during the Eocene,
1031 possibly seeded by the emplacement of particularly dense material in the lithosphere during the
1032 Late Jurassic or aided by temporal changes in the density structure of the deep crust and/or the
1033 mantle lithosphere. A second possibility is that after the Late Jurassic, the thinned lithosphere was
1034 maintained via shear-driven upwelling until the present day, and there was an episode during the
1035 Eocene that involved either enhanced melt production or processes in the crust, perhaps involving
1036 a reorganization of the regional stress field, that allowed melt to reach the surface. Specifically, a
1037 change in plate motion may have enabled a pulse of particularly intense upwelling in the
1038 lithospheric divot during the Eocene, producing unusually large volumes of partial melt.
1039 Alternatively, a change in plate motion may have coincided with a reorganization of crustal
1040 stresses, allowing for partial melt that was already present in the uppermost mantle to find its way
1041 to the surface. In either case, we suggest that the most likely scenario since the Eocene is that the
1042 CAA lithospheric divot, whether it was created in its current form during the Late Jurassic or
1043 during the Eocene, has been maintained through small-scale mantle flow and shear-driven
1044 upwelling as the North American plate has continued to move over the underlying upper mantle.
1045 While the scenarios shown in Figure 8 generally match the observations summarized in
1046 this paper, and seem to be geodynamically plausible (e.g., Conrad & Molnar, 1997; Conrad et al.,
1047 2010, 2011), there are still some aspects of the observations that are not well explained. The origin
1048 and implications of a conductivity anomaly in the deep upper mantle documented by Evans et al.
1049 (2019) remain obscure. It is difficult to explain the lack of a present-day heat flow anomaly, and

the presence of normal (as opposed to slow) crustal velocities above the thin lithosphere, if the lithospheric divot has been maintained over 50 Myr or more of geologic time. Furthermore, the controls on the timing of the second (Eocene) magmatic pulse remain poorly understood; whether triggered by a second episode of lithospheric foundering or by an intense pulse of shear-driven upwelling, we do not have a good understanding of what might have controlled the timing of the second event.

Two non-exclusive possibilities can explain the apparent occurrence of a "headless" melting column (that is, the presence of partial melt in the uppermost mantle today with a lack of contemporaneous volcanism). First, present-day melt fractions could be too low beneath the remnant lithosphere to produce an eruption. Experimental constraints on the combined effects of melt-generation, the *in-situ* melt, and volatiles (Gaillard et al., 2008; Takei, 2017; Sifré et al., 2014; Yamauchi & Takei, 2016; Yoshino et al., 2010) suggest that geophysical anomalies could be explained by small, perhaps infinitesimal, melt fractions. Second, the remnant continental lithosphere and cold crust above the CAA may be essentially impermeable, such that any partial melt present in the shallow asthenosphere today cannot make its way to the surface. Under either condition, this portion of the passive margin of North America hosts a supra-solidus uppermost mantle with no present-day volcanic activity, and therefore represents a fascinating case study to understand the behavior of partial melt in the asthenosphere.

8. Discussion and conclusions

8.1 Unanswered questions and avenues for future work

A major outstanding question regarding the lithospheric loss event(s) beneath the Central Appalachians is to what extent the lower crust was involved, and whether the crustal density

structure is important in driving lithospheric loss. As discussed above, there are some indications that the lower crust above the CAA today is denser than typical continental crust. One argument for excess density today comes from the particularly deep Moho beneath the mountains (Long et al., 2019), which may be explained by time-progressive metamorphic reactions in the roots of old mountain belts (Fischer, 2002). There are also observations of garnet-rich lower crustal xenoliths in Late Jurassic magmatic rocks above the CAA (Johnson et al., 2013), although it is not clear to what extent this observation might inform our view of lower crustal density either today or during the Eocene lithospheric loss event. One possible scenario is that particularly dense material was emplaced in the lower portion of the crust during the Late Jurassic and Eocene magmatic events. The emplacement of particularly dense (and seismically fast) material in the lower crust associated with volcanism at the surface has been inferred elsewhere in eastern North America, specifically in Mesozoic rift basins that host CAMP volcanics; examples include the South Georgia Basin (Marzen et al., 2020) and the Hartford Basin (Gao et al., 2020). Regardless of the source of the high-density material, the question of whether, and to what extent, the density structure of the lower crust plays a role in controlling lithospheric loss events is an important one. Some modeling work on catastrophic lithospheric loss has demonstrated that the lower crust, in addition to the lithospheric mantle, can be removed, and excess density in the lower crust can act as a driver for Rayleigh-Taylor instabilities (e.g., Krystopowicz & Currie, 2013). In other models of lithospheric instabilities, however, only the lower portion of the mantle lithosphere is involved (e.g., Conrad & Molnar, 1997). Future modeling work that is specific to the Central Appalachians and that considers a full suite of possible lithospheric density and rheology structure may help us to understand whether the lower crust was likely involved in past lithospheric loss event(s) and may

make specific and testable predictions about the kind of lithospheric structures that should be expected today.

A key outstanding question, and a compelling target for future work, is to understand whether the observations that are not obviously consistent with the preferred model presented in Section 7.2 can in fact be reconciled with it. Our preferred scenario (Figure 8) makes a few predictions that are not particularly consistent with the data. First, it remains somewhat unclear why there is no obvious, pronounced gravity anomaly associated with the CAA (Figure 5), if the CAA is indeed associated with the removal of dense continental lithosphere and its replacement with (perhaps continuously upwelling) less dense asthenospheric upper mantle. This question can likely be resolved in the future with detailed gravity modeling that takes into account the fine-scale details of crustal structure that have been resolved using MAGIC data. Second, if the lithosphere in the CAA region is indeed thin, and small-scale mantle flow is continuously driving upwelling in the mantle "divot" that brings relatively hot asthenosphere into contact with the base of a thin lithosphere, then it is unclear why there is no clear signature of elevated heat flow in the region. Third, if shear-driven upwelling has persisted since (at least) the Eocene, then one might expect a thermal anomaly, and thus relatively low seismic velocities, in the crust above the CAA; however, none of the tomographic models show a clear crustal velocity anomaly (Figure 3). A fourth apparent paradox stems from the fact that we observe elevated erosion rates in the CAA region today (Figure 7), and we can infer that they have either persisted since a hypothesized Eocene lithospheric removal event, or (more likely) reflect ongoing processes (small-scale mantle flow and shear-driven upwelling) that have themselves persisted since at least the Eocene. Despite the relatively fast erosion rates in the CAA region, however, we do not observe relatively thin crust, as one might expect from a prolonged period of fast erosion and associated isostatic adjustment.

Another unsolved problem that represents a compelling target for future work is the question of how general the processes of lithospheric loss and evolution that we propose for the Central Appalachians might be. Is this set of processes specific to the Central Appalachians, or might they operate more broadly beneath passive continental margins, and thus play an important role in the evolution of continental lithosphere in a passive margin setting? If the former, then what are the aspects of the structure and evolution of the Central Appalachians that have led to its unusual lithospheric modification? If the latter, then can we see evidence for similar lithospheric evolution, either ongoing or in the recent past, in passive margin settings, and what does it imply for our understanding of how continental lithosphere evolves more generally?

8.2 Summary

There are several independent lines of evidence for lithospheric loss beneath the Central Appalachian Mountains in the geologic past. The lithosphere associated with the CAA today is thin (likely < 80 km thick), as evidenced by geophysical anomalies in the upper mantle, including slow seismic velocities, high seismic attenuation, and high electrical conductivity. Receiver function imaging of the lithosphere-asthenosphere boundary is also consistent with a thin lithosphere beneath the Central Appalachians. These geophysical anomalies are co-located with a region of particularly high erosion rates; these may be linked directly to the lithospheric loss event(s), and/or may result from ongoing processes that maintain the thin lithosphere, such as shear-driven upwelling. There are two distinct episodes of intraplate magmatic activity that post-date the last major tectonic event (the breakup of Pangea), with one pulse of magmatism during the Late Jurassic and one during the Eocene. Geochemical and petrological investigation of the Late Jurassic and Eocene magmatic products provide constraints on the conditions of melting. We

have articulated and evaluated a suite of conceptual models for lithospheric loss beneath the Central Appalachians and find support for a class of models that invoke either episodic lithospheric loss via Rayleigh-Taylor instabilities, or a Rayleigh-Taylor instability followed by small-scale convection and an episode of enhanced mantle upwelling driven by shearing. The thin lithosphere beneath the Central Appalachians has likely been maintained since the last episode of magmatic activity through processes that include small-scale mantle flow and/or shear-driven upwelling. While the exact mechanisms for lithospheric loss and intraplate volcanism beneath the Central Appalachians remain imperfectly understood, our synthesis has laid out what aspects of the present-day structure and the geochemical and petrological characteristics of the magmatic products are well understood, and what aspects still need to be studied. We have articulated several avenues for future work that may help to discriminate among the plausible models for the evolution of the Central Appalachian lithosphere. In particular, future modeling studies that seek to evaluate the conceptual models we propose here in a quantitative and regionally specific framework will help to evaluate their plausibility and consistency with observations in detail.

Acknowledgements

This work benefited from discussions at the EarthScope Synthesis Workshop on the Evolution of the Southern Appalachian Lithosphere, held at Brown University in March 2017. We acknowledge support from the U.S. National Science Foundation via grants EAR-1460257 (RLE), EAR-1249412 (EG), EAR-1249438 (EAJ), EAR-1250988 (SDK), EAR-1251538 (EK), and EAR-1251515 (MDL). We thank Randy Keller for making the PACES gravity data available. The collection and dissemination of most of the geophysical data and models discussed in this paper were facilitated by the Incorporated Research Institutions for Seismology (IRIS). The facilities of

the IRIS Consortium are supported by the U.S. National Science Foundation under Cooperative Agreement EAR-1261681.

Data Availability Statement

No new data were generated as part of this study. Data from previously published sources that were used in this work are available through Duxbury et al. (2015), Long et al. (2020), Mazza et al. (2014, 2017), Perry et al. (1979), Portenga and Bierman (2011), and Portenga et al. (2019). Seismic and magnetotelluric data that underpin the geophysical models are available through the IRIS Data Management Center (https://ds.iris.edu/ds/nodes/dmc/). Many of the tomographic models are available through the IRIS Earth Model Collaboration (http://ds.iris.edu/ds/products/emc/).

References

Abers, G.A., Fischer, K.M., Hirth, G., Wiens, D.A., Plank, T., Holtzman, B.K., et al. (2014). Reconciling mantle attenuation-temperature relationships from seismology, petrology, and laboratory measurements. *Geochemistry, Geophysics, Geosystems, 15*, 3521–3542. https://doi.org/10.1002/ 2014GC005444.

Aragon, J. C., Long, M. D., & Benoit, M. H. (2017). Lateral variations in SKS splitting across the MAGIC array, central Appalachians. *Geochemistry, Geophysics, Geosystems, 18,* 4136-4155. https://doi.org/10.1002/2017GC007169.

Bailey, D. G., & Lupulescu, M.V. (2015). Spatial, temporal, mineralogical, and compositional variations in Mesozoic kimberlitic magmatism in New York State. *Lithos*, 212, 298–310. https://doi.org/10.1016/j.lithos.2014.11.022

Baba, K., Chave, A. D., Evans, R. L., Hirth, G., & Mackie, R. L. (2006a). Mantle dynamics beneath the East Pacific Rise at 17°S: Insights from the Mantle Electromagnetic and Tomography (MELT) experiment. *Journal of Geophysical Research: Solid Earth*, *111*(B2), B02101. https://doi.org/10.1029/2004JB003598.

Baba, K., Tarits, P., Chave, A. D., Evans, R. L., Hirth, G., & Mackie, R. L. (2006b). Electrical structure beneath the northern MELT line on the East Pacific Rise at 15°45'S. *Geophysical Research Letters, 33*, L22301. https:doi.org/10.1029/2006GL027528.

Babikoff, J.C., & Dalton, C.A. (2019). Long-period Rayleigh wave phase velocity tomography using USArray. *Geochemistry, Geophysics, Geosystems*, *20*(4), 1990-2006. https://doi.org/10.1029/2018GC008073.

Ballmer, M. D., Conrad, C. P., Smith, E. I., & Johnsen, R. (2015). Intraplate volcanism at the edges of the Colorado Plateau sustained by a combination of triggered edge-driven convection and shear-driven upwelling. *Geochemistry, Geophysics, Geosystems, 16,* 366-379. https://doi.org/10.1002/2014GC005641.

Baldwin, J. A., Whipple, K. X., & Tucker, G. E. (2003). Implications of the shear stress river incision model for the timescale of postorogenic decay of topography. *Journal of Geophysical Research: Solid Earth, 108*(B3), 2158. https://doi.org/10.1029/2001JB000550.

Benoit, M. H., Long, M. D., & King, S. D. (2013), Anomalously thin transition zone and apparently isotropic upper mantle beneath Bermuda: Evidence for upwelling. *Geochemistry, Geophysics, Geosystems, 14*, 4282-4291. https://doi.org/10.1002/ggge.20277.

Bensen, G.D., Ritzwoller, M.H., & Shapiro, N.M. (2008). Broadband ambient noise surface wave tomography across the United States. *Journal of Geophysical Research: Solid Earth, 113*, B05306. https://doi.org/10.1029/2007JB005248.

Bezada, M.J. (2017). Insights into the lithospheric architecture of Iberia and Morocco from teleseismic body-wave attenuation. *Earth and Planetary Science Letters, 478*, 14–26. https://doi.org/10.1016/j.epsl.2017.08.029.

Bezada, M.J., Byrnes, J., & Eilon, Z. (2019). On the robustness of attenuation measurements on teleseismic P waves: insights from micro-array analysis of the 2017 North Korean nuclear test. *Geophysical Journal International, 218*, 573 – 585. https://doi.org/10.1093/gji/ggz169.

Bikerman, M., Prellwitz, H. S., Dembosky, J., Simonetti, A., &Bell, K. (1997). New phlogopite K-Ar dates and the age of southwestern Pennsylvania kimberlite dikes. *Northeastern Geology and Environmental Sciences,* 19, 302-308.

Bina, C. R., & Helffrich, G. (1994). Phase transition Clapeyron slopes and transition zone seismic discontinuity topography. *Journal of Geophysical Research: Solid Earth, 99,* 15,853 – 15,860. https://doi.org/10.1029/94JB00462.

Birch, F. (1961). The velocity of compressional waves in rocks to 10 kilobars, Part 2. *Journal of Geophysical Research: Solid Earth, 66*, 2199-2224. https://doi.org/10.1029/JZ066i007p02199.

Biryol, C. B., Wagner, L. S., Fischer, K. M., & Hawman, R.B. (2016). Relationship between observed upper mantle structures and recent tectonic activity across the Southeastern United States. *Journal of Geophysical Research: Solid Earth, 121*(5), 3393-3414. https://doi.org/10.1022/2015JB012698.

Blackburn, T. J., Olsen, P. E., Bowring, S. A., McLean, N. M., Kent, D. V., Puffer, J., McHone, G., Rasbury, E. T., & Et-Touhami, M. (2013). Zircon U-Pb geochronology links the end-Triassic extinction with the Central Atlantic Magmatic Province. *Science, 340*, 941-945. https://doi.org/10.1126/science.1234204.

Blackman, D. K., & Kendall, J.-M. (2002). Seismic anisotropy in the upper mantle: 2. Predictions for current plate boundary flow models. *Geochemistry, Geophysics, Geosystems, 3,* 1-26. https://doi.org/20.1029/2001GC000247.

Boyce, A., Bastow, I. D., Golos, E. M., Rondenay, S., Burdick, S., & Van der Hilst, R.D. (2019). Variable modification of continental lithosphere during the Proterozoic Grenville orogeny: Evidence from teleseismic P-wave tomography. *Earth and Planetary Science Letters, 525*, 115763. https://doi.org/10.1016/j.epsl.2019.115763.

Burton, W.C., & Southworth, S. (2010). A model for Iapetan rifting of Laurentia based on Neoproterozoic dikes and related rocks, *in* Tollo, R. P., Bartholomew, M. J., Hibbard, J. P., &

Karabinos, P.M., eds., From Rodinia to Pangea: The Lithotectonic Record of the Appalachian Region, Geological Society of America, Boulder, CO, Memoir 206, pp. 455-476.

Byrnes, J. S., Bezada, M., Long, M. D., & Benoit, M. H. (2019). Thin lithosphere beneath the central Appalachian Mountains: Constraints from seismic attenuation beneath the MAGIC array. *Earth and Planetary Science Letters, 519,* 297-307. https://doi.org/10.1016/j.epsl.2019.04.045.

Callegaro, S., Marzoli, A., Bertrand, H., Chiaradia, M., Reisberg, L., Meyzen, C., et al. (2013). Upper and lower crust recycling in the source of CAMP basaltic dykes from southeastern North America. *Earth and Planetary Science Letters*, 376, 186–199. https://doi.org/10.1016/j.epsl.2013.06.023

Chu, R., Leng, W., Helmberger, D. V., & Gurnis, M. (2013). Hidden hotspot track beneath the eastern United States. *Nature Geoscience, 6,* 963-966. https://doi.org/10.1038/NGEO1949.

Conrad, C. P., Wu, B., Smith, E. I., Bianco, T. A., & Tibbetts, A. (2010). Shear-driven upwelling induced by lateral viscosity variations and asthenospheric shear: A mechanism for intraplate volcanism. *Physics of the Earth and Planetary Interiors, 178,* 162-175. https://doi.org/10.1016/j.pepi.2009.10.001.

Conrad, C. P., Bianco, T. A., Smith, E. I., & Wessel, P. (2011). Patterns of intraplate volcanism controlled by asthenospheric shear. *Nature Geoscience, 4,* 317-321. https://doi.org/10.1038/ngeo1111.

Conrad, C. P., & Molnar, P. (1997). The growth of Rayleigh-Taylor-type instabilities in the lithosphere for various rheological and density structures. *Geophysical Journal International, 129,* 95-112. https://doi.org/10.1111/j.1365-246X.1997.tb00939.x.

Cook, F. A. (1984). Towards and understanding of the southern Appalachian Piedmont crustal transition – A multidisciplinary approach. *Tectonophysics, 109,* 77-92. https://doi.org/10.1016/0040-1951(84)90171-9.

Davis, W.M. (1889). The rivers and valleys of Pennsylvania. *National Geographic Magazine 1*, 183-253.

DiBiase, R.A., Denn, A.R., Bierman, P.R., Kirby, E., West, N., & Hidy, A.J. (2018). Stratigraphic control of landscape response to base-level fall, Young Womans Creek, Pennsylvania, USA. *Earth and Planetary Science Letters*, *504*, 263-173, https://doi.org/10.1016/j.epsl.2018.10.005.

DiBiase, R.A., & Whipple, K.X. (2011). The influence of erosion thresholds and runoff variability on the relationships among topography, climate, and erosion rate. *Journal of Geophysical Research: Earth Surface, 116*, F04036. https://doi.org/10.1029/2011JF002095.

DiBiase, R.A., Whipple, K.X., Heimsath, A.M., & Ouimet, W.B. (2010). Landscape form and millennial erosion rates in the San Gabriel Mountains, CA. *Earth and Planetary Science Letters, 289*, 134-144. https://doi.org/10.1016/j.epsl.2009/10.036.

Dicken, C. L., Nicholson, S. W., Horton, J.D., Kinney, S. A., Gunther, G., Foose, M. P., & Mueller, J. A. L. (2005). Preliminary integrated geologic map databases for the United States: Delaware, Maryland, New York, Pennsylvania, and Virginia. U.S. Geological Survey Open File Report 2005-1325, accessed January 31, 2013, at https://pubs.usgs.gov/of/2005/1325.

Dong, M. T., & Menke, W. H. (2017). Seismic high attenuation region observed beneath southern New England from teleseismic body wave spectra: Evidence for high asthenospheric temperature without melt. *Geophysical Research Letters, 44,* 10,958-10,969. https://doi.org/10.1002/2017GL074953.

Duxbury, J., Bierman, P. R., Portenga, E. W., Pavich, M. J., Southworth, S., & Freeman, S. P. (2015). Erosion rates in and around Shenandoah National Park, Virginia, determined using analysis of cosmogenic 10Be. *American Journal of Science, 315,* 46-76. https://doi.org/10.2475/01.2015.02.

Dziewonski, A.M. & Anderson, D.L. (1981). Preliminary Reference Earth Model. *Physics of the Earth and Planetary Interiors, 25*(4), 297-356. https://doi.org/10.1016/0031-9201(81)90046-7.

Eilon, Z. C., & Abers, G. A. (2017). High seismic attenuation at a mid-ocean ridge reveals the distribution of deep melt. *Science Advances, 3*(5), e1602829. https://doi.org/10.126/sciadv.1602829.

Elkins-Tanton, L. T. (2007). Continental magmatism, volatile recycling, and a heterogeneous mantle caused by lithospheric gravitational instabilities. *Journal of Geophysical Research: Solid Earth, 112,* B03405. https://doi.org/10.1029/2005JB004072.

Evans, R. R., Benoit, M. H., Long, M. D., Elsenbeck, J., Ford, H. A., Zhu, J., & Garcia, X. (2019). Thin lithosphere beneath the central Appalachian Mountains: A combined seismic and magentotelluric study. *Earth and Planetary Science Letters, 519,* 308-316. https://doi.org/10.1016/j.epsl.2019.04.46.

Fernandes, V. M., Roberts, G. G., White, N., & Whittaker, A. C. (2019). Continental-scale landscape evolution: A history of North American topography. *Journal of Geophysical Research: Earth Surface, 124*(11), 2689-2722. https://doi.org/10.1029/2018JF004979.

Fischer, K.M. (2002). Waning buoyancy in the crustal roots of old mountains. *Nature, 417,* 933–936. https://doi.org/10.1038/nature00855.

Foland, K., Gilbert, L. A., Sebring, C. A., & Jiang-Feng, C. (1986). 40Ar/39Ar ages for plutons of the Monteregian Hills, Quebec: Evidence for a single episode of Cretaceous magmatism. *Geological Society of America Bulletin, 97*(8), 966–974. https://doi.org/10.1130/0016-7606(1986)97.

Foland, K. A., Quinn, A. W., & Giletti, B. J. (1971). K-Ar and Rb-Sr Jurassic and Cretaceous ages for intrusives of the White Mountain magma series, northern New England. *American Journal of Science,* 270(5), 321-330. https://doi.org/10.2475/ajs.270.5.321.

Frone, Z. S., Blackwell, D. D., Richards, M. C., & Hornbach, M. J. (2015). Heat flow and thermal modeling of the Appalachian Basin, West Virginia. *Geosphere, 11*(5), 1279-1290. https://doi.org/10.1130/GES01155.1.

Gaillard, F., Malki, M., Iacono-Marziano, G., Pichavant, M., & Scaillet, B. (2008). Carbonatite melts and electrical conductivity in the asthenosphere. *Science, 322,* 1363-1365. https://doi.org/10.1126/science.1164446.

Gallen, S.F. (2018). Lithologic controls on landscape dynamics and aquatic species evolution in post-orogenic mountains. *Earth and Planetary Science Letters, 493,* pp.150-160. https://doi.org/10.1016/j.epsl/2018.04.029.

Gallen, S. F., Wegmann, K. W., & Bohnenstiehl, D. R. (2013). Miocene rejuvenation of topographic relief in the southern Appalachians. *GSA Today, 23,* 4-10. https://doi.org/10.1130/GSATG163A.1.

Gao, S. S., & Liu, K. H. (2014). Mantle transition zone discontinuities beneath the contiguous United States. *Journal of Geophysical Research: Solid Earth, 119,* 6452-6468. https://doi.org/10.1002.2014JB011253.

Gao, H., Yang, X., Long, M. D., & Aragon, J. C. (2020). Seismic evidence for crustal modification beneath the Hartford Rift Basin in the Northeastern United States. *Geophysical Research Letters*, 47, e2020GL089316. https://doi.org/10.1029/2020GL089316.

Golos, E.M., Fang, H., Yao, H., Zhang, H., Burdick, S., Vernon, F., et al. (2018). Shear wave tomography beneath the United States using a joint inversion of surface and body waves. *Journal of Geophysical Research: Solid Earth*, *123*(6), 5169-5189. https://doi.org/ 10.1029/2017JB014894.

Goren, L., Fox, M., & Willett, S.D. (2014). Tectonics from fluvial topography using formal linear inversion: Theory and applications to the Inyo Mountains, California. *Journal of Geophysical Research: Earth Surface, 119*, 1651-1681. https://doi.org/10.1002/2014JF003079.

Gripp, A. E., & Gordon, R. G. (2002). Young tracks of hotspots and current plate velocities. *Geophysical Journal International*, *150*(2), 321-361. https://doi.org/10.1046/j.1365-246X.2002.01627.x.

Griscom, A. (1963). Tectonic significance of the Bouguer gravity field of the Appalachian System. *Geological Society of America Special Paper, 73*, 163-164.

Hack, J. T. (1960). Interpretation of erosional topography in humid temperate regions. *American Journal of Science, 258*, pp.80–97.

Hancock, G., & Kirwan, M. (2007). Summit erosion rates deduced from 10Be; implications for relief production in the Central Appalachians. *Geology, 35*, 89–92. https://doi.org/10.1130/ G23147A.1.

Harkins, N., Kirby, E., Heimsath, A., Robinson, R., & Reiser, U. (2007). Transient fluvial incision in the headwaters of the Yellow River, northeastern Tibet, China. *Journal of Geophysical Research: Earth Surface, 112*, F03S04. https://doi.org/10.1029/2006JF000570.

Hatcher, Jr., R.D. (2010). The Appalachian orogeny: A brief summary, *in* Tollo, R. P., Bartholomew, M. J., Hibbard, J. P., & Karabinos, P. M., eds., From Rodinia to Pangea: The Lithotectonic Record of the Appalachian Region, Geological Society of America, Boulder, CO, Memoir 206, pp. 1-19.

Havlin, C., Parmentier, E. M., & Hirth, G (2013). Dike propagation driven by melt accumulation at the lithosphere–asthenosphere boundary. *Earth and Planetary Science Letters, 376*, 20-28. https://doi.org/10.1016/j.epsl.2013.06.010.

Haynes, J. T., Johnson, E. A., & Whitmeyer, S. J. (2014). Active features along a "passive" margin: The intriguing interplay between Silurian-Devonian stratigraphy, Alleghanian deformation, and Eocene magmatism of Highland and Bath Counties, Virginia, *in* Bailey, C. M., & Coiner, L.V., eds., Elevating Geoscience in the Southeastern United States: New Ideas about Old Terranes: Field Guides for the GSA Southeastern Section Meeting, Blacksburg, Virginia, 2014. Geological Society of America Field Guide 35, 1-40, https://doi.org/10.1130/2014.0035(01).

Hibbard, J. P., van Staal, C. R., & Rankin, D. W. (2010). Comparative analysis of the geological evolution of the northern and southern Appalachian orogeny: Late Ordovician-Permian, *in* Tollo, R. P., Bartholomew, M. J., Hibbard, J. P., & Karabinos, P. M., eds., From Rodinia to Pangea: The Lithotectonic Record of the Appalachian Region, Geological Society of America, Boulder, CO, Memoir 206, pp. 51-69.

Hutchinson, D. R., Klitgord, K. D., & Detrick, R. S. (1986). Rift basins of the Long Island platform. *Geological Society of America Bulletin, 97*, 688-702. https://doi.org/10.1130/0016-7606(1986)97<688:RBOTLI>2.0.CO;2.

Ito, G., Dunn, R., & Li, A. (2015). The origin of shear wave splitting beneath Iceland. *Geophysical Journal International, 201*, 1297-1312. https://doi.org/10.1093/gji/ggv078.

Jacobsen, B. H. (1987). A case for upward continuation as a standard separation filter for potential-field maps. *Geophysics, 52,* 1033-1165. https://doi.org/10.1190/1.1442378.

Johnson, R. W., Milton, C., & Dennison, J. M. (1971). Field trip to the igneous rocks of Augusta, Rockingham, Highland, and Bath counties, Virginia. *Virginia Division of Mineral Resources*, 16, 1–68.

Johnson, E. A., Kiracofe, Z. A., Haynes, J. T., & Nashimoto, K. (2013). The origin of sandstone xenoliths in the Mole Hill basalt, Rockingham County, Virginia: Implications for magma ascent and crustal structure in the western Shenandoah Valley. *Southeastern Geology*, 49, 95–118.

Kaislaniemi, L., & van Hunen, J. (2014). Dynamics of lithospheric thinning and mantle melting by edge-driven convection: Application to Moroccan Atlas mountains. *Geochemistry, Geophysics, Geosystems, 15*, 3175-3189. https://doi.org/10.1002/2014GC005414.

Karner, G. D., & Watts, A. B. (1983). Gravity anomalies and flexure of the lithosphere at mountain ranges. *Journal of Geophysical Research: Solid Earth, 88*(B12), 10449-10477. https://doi.org/10.1029/JB088uB12p10449.

Keifer, I., & Dueker, K. (2019). Testing the hypothesis that temperature modulates 410 and 660 discontinuity topography beneath the eastern United States. *Earth and Planetary Science Letters, 524,* 115723. https://doi.org/10.1016/j.epsl.2019.115723.

Kennett, B. L. N., & Engdahl, E. R. (1991). Traveltimes for global earthquake location and phase identification. *Geophysical Journal International, 105*, 429-465. https://doi.org/10.1111/j.13640246X.1991.tb06724.x.

Key, K., Constable, S., Liu, L., & Pommier, A. (2013). Electrical image of passive mantle upwelling beneath the northern East Pacific Rise. *Nature, 495,* 499-502. https://doi.org/10.1038/nature11932.

King, S.D. (2007), Hotspots and edge-driven convection. *Geology, 35,* 223-226. https://doi.org/10.1130/G23291A.1.

King, S. D., & Anderson, D. L. (1998). Edge-driven convection. *Earth and Planetary Science Letters, 160,* 289-296. https://doi.org/10.1016/S0012-821X(98)00089-2.

Kinney, S., Maclennan, S. A., Setera, J., Schoene, B., VanTongeren, J., Strauss, J. V., et al. (2020). Long-lived and localized post-orogenic magmatism on the eastern North American margin: insights from zircon U-PB geochronology. *Geological Society of America Abstracts with Programs,* 10.1130/abs/2020SE-345449.

Kirby, E., & Whipple, K. X. (2012). Expression of active tectonics in erosional landscapes. *Journal of Structural Geology, 44*, 54-75. https://doi.org/10.1016/j.jsg.2012.07.009.

Krystopowicz, N. J., & Currie, C. A. (2013). Crustal eclogitization and lithospheric delamination in orogens. *Earth and Planetary Science Letters, 361,* 195-207. https://doi.org/10.1016/j.epsl/2012.09.056.

Lague, D. (2014). The stream power river incision model: evidence, theory and beyond. *Earth Surface Processes and Landforms, 39*, 38-61. http://doi.org/10.1002/esp.3462.

Lekic, V., & Romanowicz, B. (2011). Tectonic regionalization without a priori information: A cluster analysis of upper mantle tomography. *Earth and Planetary Science Letters, 308,* 151–160. https://doi.org/10.1016/j.epsl.2011.05.050.

Levandowski, W., Hermann, R. B., Briggs, R., Boyd, O., & Gold, R. (2018). An updated stress map of the continental United States reveals heterogeneous intraplate stress. *Nature Geoscience, 11,* 433-437. https://doi.org/10.1038/s41561-018-0120-x.

Levin, V., Long, M. D., Skryzalin, P., Li, Y., & López, I. (2018). Seismic evidence for a recently formed mantle upwelling beneath New England. *Geology, 46,* 87-90. https://doi.org/10.1130/G39641.1.

Li, C., Gao, H., & Williams, M. L. (2020). Seismic characteristics of the eastern North American crust with Ps converted waves: Terrane accretion and modification of continental crust. *Journal of Geophysical Research: Solid Earth, 125,* e2019JB018727. https://doi.org/ 10.1029/2019JB018727.

Li, Z. X., Bogdanova, S.V., Collins, A.S., Davison, A., De Waele, B., Ernst, R.E., et al. (2008). Assembly, configuration, and break-up history of Rodinia: A synthesis. *Precambrian Research, 160,* 179-210. https://doi.org/10.1016/j.precamres.2007.04.021.

Lin, F.-C., Ritzwoller, M. H., & Snieder, R. (2009). Eikonal tomography: Surface wave tomography by phase-front tracking across a regional broad-band seismic array. *Geophysical Journal International, 177,* 1091–1110. https://doi.org/10.1111/j.1365-246X.2009.04105.x.

Lin, F. C., & Ritzwoller, M. H. (2011). Helmholtz surface wave tomography for isotropic and azimuthally anisotropic structure. *Geophysical Journal International, 186,* 1104–1120. https://doi.org/10.1111/j.1365-246X.2011.05070.x.

Liu, L. (2014). Rejuvenation of Appalachian topography caused by subsidence-induced differential erosion. *Nature Geoscience, 7,* 518-523. https://doi.org/10.1038/NGEO2187.

Liu, S., Aragon, J. C., Benoit, M. H., Long, M. D., & King, S. D. (2018). Transition zone structure beneath the eastern U.S. *AGU Fall Meeting,* Washington, DC, abstract T52D-05.

Liu, Y., & Holt, W. E. (2015). Wave gradiometry and its link with Helmholtz equation solutions applied to USArray in the eastern US. *Journal of Geophysical Research: Solid Earth, 120,* 5717–5746. https://doi.org/10.1002/2015JB011982.

Long, L. T. (1979). The Carolina slate belt – Evidence of a continental rift zone. *Geology, 7,* 180-184. https://doi.org/10.1130/0091-7613(1979)7<180:TCSBOA>2.0.CO;2.

Long, M. D., Benoit, M. H., Chapman, M. C., & King, S. D. (2010). Upper mantle anisotropy and transition zone thickness beneath southeastern North America and implications for mantle dynamics. *Geochemistry, Geophysics, Geosystems, 11,* Q10012. https://doi.org10.1029/ 2010GC003247.

Long, M. D., Jackson, K. G., & McNamara, J. F. (2016). *SKS* splitting beneath Transportable Array stations in eastern North America and the signature of past lithospheric deformation. *Geochemistry, Geophysics, Geosystems, 17,* 2-15. https://doi.org/10.1029/2015GC006088.

Long, M. D., Benoit, M. H., Aragon, J. C., & King, S. D. (2019). Seismic imaging of mid-crustal structure beneath central and eastern North America: Possibly the elusive Grenville deformation? *Geology, 47,* 371-374. https://doi.org/10.1130/G46077.1.

Long, M. D., Benoit, M. H., Evans, R. L., Aragon, J. C., & Elsenbeck, J. (2020). The MAGIC experiment: A combined seismic and magnetotelluric deployment to investigate the structure, dynamics, and evolution of the central Appalachians. *Seismological Research Letters, 91,* 2960-2975. https://doi.org/10.1785/0220200150.

Magni, V., & Király, Á. (2020). Delamination. *Reference Module in Earth Systems and Environmental Sciences,* Elsevier. https://doi.org/10.1016/B978-0-12-409548-9.09515-4.

Marzen, R. E., Shillington, D. J., Lizarralde, D., Knapp, J. H., Heffner, D. M., Davis, J. K., & Harder, S. H. (2020). Limited and localized magmatism in the Central Atlantic Magmatic Province. *Nature Communications, 11,* 3397. https://doi.org/10.1038/s41467-020-17193-6.

Marzoli, A., Callegaro, S., Dal Corso, J., Davies, J. H. F. L., Chiaradia, M., Youbi, N., et al. (2018). The Central Atlantic Magmatic Province (CAMP): A review. In: Tanner, L. H., ed., *The Late Triassic World, Topics in Geobiology*, vol. 46, pp. 91-125. New York, NY: Springer.

Matmon, A., Bierman, P. R., Larsen, J., Southworth, S., Pavich, M. J., & Caffee, M. W. (2003). Temporally and spatially uniform rates of erosion in the southern Appalachian Great Smoky Mountains. *Geology, 31*, 155-158. https://doi.org/10.1130/0091-7613(2003)031<0155:TASURO>2.0.CO;2.

Mazza, S. E., Gazel, E. A., Johnson, E. A., Bizimis, M., McAleer, R., & Biryol, C. B. (2017). Post-rift magmatic evolution of the eastern North American "passive-aggressive" margin. *Geochemistry, Geophysics, Geosystems, 18*, 3-22, https://doi.org/10.1002/2016GC006646.

Mazza, S. E., Gazel, E., Johnson, E. A., Kunk, M. J., McAleer, R., Spotila, J. A., Bizimis, M., & Coleman, D. S. (2014). Volcanoes of the passive margin: The youngest magmatic event in eastern North America. *Geology, 42*, 483-486. https://doi.org/10.1130/G35407.1.

McHone, J. G. (1996), Constraints on the mantle plume model for Mesozoic alkaline intrusions in northeastern North America. *Canadian Mineralogist*, 34, 325–334.

McLelland, J. M., Selleck, M. W., & Bickford, M. E. (2010). Review of the Proterozoic evolution of the Grenville Province, its Adirondack outlier, and the Mesoproterozoic inliers of the Appalachians, *in* Tollo, R.P., Bartholomew, M. J., Hibbard, J. P., & Karabinos, P. M., eds., From Rodinia to Pangea: The Lithotectonic Record of the Appalachian Region, Geological Society of America, Boulder, CO, Memoir 206, pp. 21-49.

Menke, W., Skryzalin, P., Levin, V., Harper, T., Darbyshire, F., & Dong, T. (2016). The Northern Appalachian Anomaly: A modern asthenospheric upwelling. *Geophysical Research Letters, 43*, 10,173-10,179, https://doi.org/10.1002/2016GL070918.

Menke, W., Lamoureux, J., Abbott, D., Hopper, E., Hutson, D., & Marrero, A. (2018). Crustal heating and lithospheric alteration and erosion associated with asthenospheric upwelling beneath southern New England (USA). *Journal of Geophysical Research: Solid Earth, 123(10)*, 8995-9008. https://doi.org/10.1029/2018JB015921.

Miller, S. R., Sak, P. B., Kirby, E., & Bierman, P. R. (2013). Neogene rejuvenation of central Appalachian topography: Evidence for differential rock uplift from stream profiles and erosion rates. *Earth and Planetary Science Letters*, *369*, 1-12. https://doi.org/10.1016/j.epsl.2013.04.007.

Moucha, R., Forte, A. M., Mitrovica, J. X., Rowley, D. B., Quéré, S., Simmons, N. A., & Grand, S.P. (2008). Dynamic topography and long-term sea-level variations: There is no such thing as a stable continental platform. *Earth and Planetary Science Letters, 271*, 101-108. https://doi.org/10.1016/j.epsl.2008.03.056.

Moucha, R., & Ruetenik, G. A. (2017). Interplay between dynamic topography and flexure along the US Atlantic passive margin: Insights from landscape evolution modeling. *Global and Planetary Change*, *149*, 72-78. https://doi.org/10.1016/j.gloplacha.2017.01.004.

Naeser, C. W., Naeser, N. D., Newell, W. L., Southworth, S., Edwards, L.E., & Weems, R.E. (2016). Erosional and depositional history of the Atlantic passive margin as recorded in detrital zircon fission-track ages and lithic detritus in Atlantic Coastal Plain sediments. *American Journal of Science, 316*,110-160. https://doi.org/10.2475/02.2016.02.

Nicholson, S. W. D., Horton, C. L., Labay, J. D., Foose, K. A., Mueller, M. P., & Julia, A. L. (2005). Preliminary integrated geologic map databases for the United States: Kentucky, Ohio, Tennessee, and West Virginia: U.S. Geological Survey Open File Report 2005-1324, accessed January 31, 2013, at https://pubs.usgs.gov/of/2005/1324.

Pazzaglia, F. J., & Brandon, M. T. (1996). Macrogeomorphic evolution of the post-Triassic Appalachian mountains determined by deconvolution of the offshore basin sedimentary record. *Basin Research, 8,* 255-278. https://doi.org/10.1046/j.1365-2117.1996.00274.x.

Perron, J. T., & Royden, L. (2013). An integral approach to bedrock river profile analysis. *Earth Surface Processes and Landforms, 38*(6), 570-576. https://doi.org/10.1002/esp.3302.

Perry, L. D., Costain, J. K., & Geiser, P. A. (1979). Heat flow in western Virginia and a model for the origin of thermal springs in the folded Appalachians. *Journal of Geophysical Research: Solid Earth, 84*(B12), 6875-6883. https://doi.org/10.1029/JB084iB12p06875.

Pollitz, F. F., & J. A. Snoke (2010). Rayleigh-wave phase-velocity maps and three-dimensional shear-velocity structure of the western US from local non-plane surface-wave tomography. *Geophysical Journal International, 180,* 1153–1169. https://doi.org/10.1111.j.1365-246X.2009.04441.x.

Pollitz, F.F., & Mooney, W.D. (2016). Seismic velocity structure of the crust and shallow mantle of the Central and Eastern United States by seismic surface wave imaging. *Geophysical Research Letters, 43*(1), 118-126. https://doi.org/10.1002/2015GL066637.

Pommier A., Kohlstedt, D. L., Hansen, L. N., Mackwell, S., Tasaka, M., Heidelbach, F., & Leinenweber, K. (2018). Transport properties of olivine grain boundaries from electrical conductivity experiments. *Contributions to Mineralogy and Petrology, 173,* 41. https://doi.org10.1007/s00410-018-1468-z.

Portenga, E. W., & Bierman, P. R. (2011). Understanding Earth's eroding surface with 10Be. *GSA Today, 21*(8), 4-10. https://doi.org/10.1130/G111.A1.

Portenga, E. W., Bierman, P. R., Trodick, C. D., Greene, S. E., DeJong, B. D., Rood, D. H., & Pavich, M. J. (2019). Erosion rates and sediment flux within the Potomac River basin quantified over millennial timescales using beryllium isotopes. *Geological Society of America Bulletin, 131*(7-8), 1295-1311. https://doi.org/10.1130/B31840.1.

Porter, R., Liu, Y., & Holt, W.E., (2016). Lithospheric records of orogeny within the continental US. *Geophysical Research Letters,* 43, 144–153. https://doi.org/10.1002/2015GL066950

Pozgay, S. H., Wiens, D. A., Conder, J. A., Shiobara, H., & Sugioka, H. (2009). Seismic attenuation tomography of the Mariana subduction system: Implications for thermal structure, volatile distribution, and slow spreading dynamics. *Geochemistry, Geophysics, Geosystems,* 10, Q04X05. https://doilorg/10.1029/2008GC002313.

Pratt, T. L., Çoruh, C., Costain, J. K., & Glover III, L. (1988). A geophysical study of the Earth's crust in central Virginia: Implications for Appalachian crustal structure. *Journal of Geophysical Research: Solid Earth, 93,* 6649-6667. https://doi.org/10.1029/JB093iB06p06649.

Rowley, D. B., Forte, A. M., Moucha, R., Mitrovica, J. X., Simmons, N. A., & Grand, S. P. (2013). Dynamic topography change of the eastern United States since 3 million years ago. *Science, 340,*1560–1563. https://doi.org/10.1126/science.1229180

Sarafian, E., Gaetani, G. A., Hauri, E. H., & Sarafian, A. R. (2017). Experimental constraints on the damp peridotite solidus and oceanic mantle potential temperature. *Science, 355,* 942–945. https://doi.org/10.1126/science.aaj2165.

Savage, B. (2021). Body wave speed structure of Eastern North America. *Geochemistry, Geophysics, Geosystems, 22,* e2020GC009002. https://doi.org/10.1029/2020GC009002.

Savage, B., Covellone, B.M. & Shen, Y. (2017). Wave speed structure of the eastern North American margin. *Earth and Planetary Science Letters, 459,* 394-405.

Schaeffer, A.J. and Lebedev, S., 2014. Imaging the North American continent using waveform inversion of global and USArray data. *Earth and Planetary Science Letters*, *402*, pp.26-41. https://doi.org/10.1016/j.epsl.2016.11.028.

Schmandt, B., Dueker, K., Humphreys, E., & Hansen, S. (2012). Hot mantle upwelling across the 660 beneath Yellowstone. *Earth and Planetary Science Letters, 331-332,* 224-236. https://doi.org/10.1016/j.epsl.2012.03.025.

Schmandt, B., & Lin, F.-C. (2014). P and S wave tomography of the mantle beneath the United States. *Geophysical Research Letters*, 41, 6342–6349. https://doi.org/10.1002/2014GL061231.

Schmandt, B., Lin, F.-C., & Karlstrom, K.E. (2015). Distinct crustal isostasy trends east and west of the Rocky Mountain Front. *Geophysical Research Letters*, *42*(23), 10,290-10,298. https://doi.org/10.1002/2015GL066593.

Shen, W. & Ritzwoller, M.H. (2016). Crustal and uppermost mantle structure beneath the United States. *Journal of Geophysical Research: Solid Earth*, *121*(6), 4306-4342. https://doi.org/10.1002/2016JB012887.

Shorten, C. M., & Fitzgerald, P. G. (2021). Episodic exhumation of the Appalachian orogen in the Catskill Mountains (New York State, USA). *Geology, 49*(5), 571-575. https://doi.org/10.1130/G48011.1.

Sifré, D., Gardés, E., Massuyea, M., Hashim, L., Hier-Majumder, S., & Gaillard, F. (2014). The electrical conductivity during incipient melting in the oceanic low velocity zone. *Nature, 509,* 81-85. https://doi.org/10.1038/nature13245.

Smyth, J. R., & Frost, D. J. (2002). The effect of water on the 410-km discontinuity: An experimental study. *Geophysical Research Letters, 29,* 1485. https://doi.org/10.1029/2001GL014418.

Soles, B., Brennan, G., Johnson, E., Mazza, S., & Gazel, E. (2014). Variable water concentrations in the asthenospheric and lithospheric mantle underneath the Eastern United States. AGU Fall Meeting, San Francisco, CA, abstract ED31F-3491.

Southworth, C. S., Gray, K. J., & Sutter, J.S. (1993). Middle Eocene intrusive igneous rocks of the central Appalachian Valley and Ridge Province — Setting, chemistry, and implications for crustal structure. *U.S. Geological Survey Bulletin*, Report B1839-I, J1–J24.

Spasojevic, S., Liu, L., Gurnis, M., & Müller, R. D. (2008). The case for dynamic subsidence of the U.S. east coast since the Eocene. *Geophysical Research Letters, 35,* L08305. https://doi.org/10.1029/2008GL033511.

Spotila, J. A., Bank, G. C., Reiners, P. W., Naeser, C. W., Naeser, N. D., & Henika, B. S. (2004). Origin of the Blue Ridge escarpment along the passive margin of Eastern North America. *Basin Research, 16*, 41-63. https://doi.org/10.1111/j.1365-2117.2003.00219.x.

Stein, C. A., Stein, S., Merino, M., Keller, G. R., Flesch, L. M., & Jurdy, D. M. (2014). Was the Midcontinent Rift part of a successful seafloor-spreading episode? *Geophysical Research Letters, 41,* 1465-1470. https://doi.org/10.1002/2013GL059176.

Takei, Y., (2017). Effects of partial melting on seismic velocity and attenuation: A new insight from experiments. *Annual Review of Earth and Planetary Sciences, 45,* 447–470. https://doi.org/10.1146/annurev-earth-063016-015820.

Thomas, W. A., & Powell, C. A. (2017). Necessary conditions for intraplate seismic zones in North America. *Tectonics, 36,* 2903-2917. https://doi.org/10.1002/2017TC004502.

Till, C. B., Elkins-Tanton, L. T., & Fischer, K. M. (2010). A mechanism for low-extent melts at the lithosphere-asthenosphere boundary. *Geochemistry, Geophysics, Geosystems, 11*, Q10015. https://doi.org/10.1029/2010GC003234.

Tso, J.L., & Surber, J.D. (2006). Eocene igneous rocks near Monterey, Virginia; A field study. *Virginia Minerals*, 48, 25–40.
Turcotte, D. L., & Schubert, G. (2002). *Geodynamics.* Cambridge, UK: Cambridge University Press.
van der Lee, S., & A. Frederiksen (2005), Surface wave tomography applied to the North America upper mantle, in *Seismic Earth: Array Analysis of Broadband Seismograms*, edited by G. Nolet and A. Levander, pp.67-80, American Geophysical Union, Washington, DC.
Van der Lee, S., Regenauer-Lieb, K., & Yuen, D. (2008). The role of water in connecting past and future episodes of subduction. *Earth and Planetary Science Letters, 273,* 15-27, https://doi.org/10.1016/j.epsl.2008.04.041.
Van Wijk , J., Baldridge, S., van Hunen, J., Goes, S., Aster, R., Coblentz, D., Grand, S., & Ni, J. (2010). Small-scale convection at the edge of the Colorado Plateau: Implications for topography, magmatism, and evolution of Proterozoic lithosphere. *Geology, 38,* 611-614. https://doi.org/10.1130/G31031.1.
Wagner, L. S., Stewart, K., & Metcalf, K. (2012). Crustal-scale shortening structures beneath the Blue Ridge Mountains, North Carolina, USA. *Lithosphere, 4,* 242-256. https://doi.org/10.1130/L184.1.
Wagner, L. S., Fischer, K. M., Hawman, R., Hopper, E., & Howell, D. (2018). The relative roles of inheritance and long-term passive margin lithospheric evolution on the modern structure and tectonic activity in the southeastern United States. *Geosphere, 14,* 1385-1410. https://doi.org/10.1130/GES01593.1.
Wang, H., Zhao, D., Huang, Z. & Wang, L. (2019). Tomography, seismotectonics, and mantle dynamics of central and eastern United States. *Journal of Geophysical Research: Solid Earth, 124*(8), 8890-8907. https://doi.org/10.1029/2019JB017478.
Wang, Y., & Pavlis, G. L. (2016). Roughness of the mantle transition zone discontinuities revealed by high-resolution wavefield imaging. *Journal of Geophysical Research: Solid Earth, 121*(9), 6757-6778. https://doi.org/10.1002/2016JB013205.
Waring, G. A. (1965). Thermal springs of the United States and other countries of the world: A summary. *U. S. Geological Survey Professional Paper, 492.*
Wei, S., & Wiens, D. A. (2018). P-wave attenuation structure of the Lau back-arc basin and implications for mantle wedge processes. *Earth and Planetary Science Letters, 502,* 187-199. https://doi.org/10.1016/j.epsl.2018.09.005.
Wei, W., & Wiens, D. A. (2020). High bulk and shear attenuation due to partial melt in the Tonga-Lau back-arc mantle. *Journal of Geophysical Research: Solid Earth, 125,* e2019JB017527. https://doi.org/10.1029/2019JB017527.
Whalen, L., Gazel, E., Vidito, C., Puffer, J., Bizimis, M., Henika, W., & Caddick, M.J. (2015). Supercontinental inheritance and its influence on supercontinental breakup: The Central Atlantic Magmatic Province and the breakup of Pangea. *Geochemistry, Geophysics, Geosystems*, 16, 3532–3554. https://doi.org10.1002/2015GC005885.
Whipple, K.X., & Tucker, G.E. (1999). Dynamics of the stream-power river incision model: implications for height limits of mountain ranges, landscape response timescales, and research needs. *Journal of Geophysical Research: Solid Earth, 104,* 17661-17674. https://doi.org/10.1029/1999JB00120.
Whitmeyer, S., & Karlstrom, K. (2007). Tectonic model for the Proterozoic growth of North America. *Geosphere, 3,* 220-259. https://doi.org/10.1130/GES00055.1.

Wobus, C., Whipple, K. X., Kirby, E., Snyder, N., Johnson, J., Spyropolou, K., Crosby, B., & Sheehan, D. (2006). Tectonics from topography: Procedures, promise, and pitfalls, in: Willett, S. D., Hovius, N., Brandon, M. T., & Fisher, D. (Eds.), *Tectonics, Climate, and Landscape Evolution*. Geological Society of America, Boulder, Colorado, pp. 55-74.

Williams, M. L., Dumond, G., Mahan, K., Regan, S., & Holland, M. (2014). Garnet-forming reactions in felsic orthogneiss: Implications for densification and strengthening of the lower continental crust. *Earth and Planetary Science Letters, 405,* 207-219. https://doi.org/ 10.1016/j.epsl.2014.08.030.

Withjack, M. O., Schlische, R. W., & Olsen, P. E. (1998). Diachronous rifting, drifting, and inversion on the passive margin of Central Eastern North America: An analog for other passive margins. *AAPG Bulletin, 82,* 817-835.

Withjack, M. O., Schlische, R. W., & Olsen, P. E. (2012). Development of the passive margin of Eastern North America: Mesozoic rifting, igneous activity, and breakup. *Regional Geology and Tectonics: Phanerozoic Rift Systems and Sedimentary Basins, 1b*, 301-335.

Wolin, E., Stein, S., Pazzaglia, F., Meltzer, A., Kafka, A., & Berti, C. (2012). Mineral, Virginia earthquake illustrates seismicity of a passive-aggressive margin. *Geophysical Research Letters, 39,* L02305. https://doi.org/10.10129/2011GL050310.

Wright, N. M., Müller, R. D., Seton, M., & Williams, S. E. (2015). Revision of Paleogene plate motions in the Pacific and implications for the Hawaiian-Emperor bend. *Geology, 43,* 455-458. http://doi.org/10.1130/G36303.1.

Xie, J., Chu, R., & Yang, Y. (2018). 3-D upper-mantle shear velocity model beneath the contiguous United States based on broadband surface wave from ambient seismic noise. *Pure and Applied Geophysics*, *175*(10), 3403-3418. https://doi.org/10.1007/s00024-018-1881-2.

Yamauchi, H., & Takei, Y. (2016). Polycrystal anelasticity at near-solidus temperatures. *Journal of Geophysical Research: Solid Earth*, *121*, 2016JB013316. https://doi.org/10.1002/ 1202016JB013316.

Yang, Y., & Forsyth, D. W. (2006). Regional tomographic inversion of the amplitude and phase of Rayleigh waves with 2-D sensitivity kernels. *Geophysical Journal International, 166,* 1148-1160. https://doi.org/10.1111/j.1365-246X.2006.02972.x.

Yang, B. B., Liu, Y., Dahm, H., Liu, K. H., & Gao, S. S. (2017). Seismic azimuthal anisotropy beneath the eastern United States and its geodynamic implications. *Geophysical Research Letters, 44,* 2670–2678. https://doi.org/10.1002/2016GL071227.

Yoshino, T., Laumonier, M., McIsaac, E., & Katsura, T. (2010). Electrical conductivity of basaltic and carbonatite melt-bearing peridotites at high pressures: Implications for melt distribution and melt fraction in the upper mantle. *Earth and Planetary Science Letters, 295,* 593-602. https://doi.org/10.1016/j.epsl.2010.04.050.

Yuan, H., French, S., Cupillard, P., & Romanowicz, B. (2014). Lithospheric expression of geological units in central and eastern North America from full waveform tomography. *Earth and Planetary Science Letters, 402,* 176-186. https://doi.org/10.1016/j.epsl.2013.11.057.

Supporting Information References

Bierman, P., & Steig, E.J. (1996). Estimating rates of denudation using cosmogenic isotope abundances in sediment. *Earth Surface Processes and Landforms, 21,* 125-139. https://doi.org/10.1002/SICI/1096-9837(199602)21:2<125::AID-ESP511>3.0CO;2-8.

Granger, D.E., Kirchner, J.W., & Finkel, R. (1996). Spatially averaged long-term erosion rates measured from in situ-produced cosmogenic nuclides in alluvial sediment. *Journal of Geology, 104*, 249-257. https://doi.org/10.1086/629823.

Greene, C. A., Thirumalai, K., Kearney, K. A., Delgado, J. M., Schwanghart, W., Wolfenbarger, N. S., & Blankenship, D. D. (2019). The climate data toolbox for MATLAB. *Geochemistry, Geophysics, Geosystems*, *20*(7), 3774-3781. https://doi.org/10.1029/2019GC008392.

Schwanghart, W., & Scherler, D. (2014). TopoToolbox 2–MATLAB-based software for topographic analysis and modeling in Earth surface sciences. *Earth Surface Dynamics*, *2*(1), 1-7. https://doi.org/10.5194/esurf-2-1-2014.

Schwanghart, W., & Scherler, D. (2017). Bumps in river profiles: uncertainty assessment and smoothing using quantile regression techniques. *Earth Surface Dynamics*, *5*, 821-839. https://doi.org/10.5194/esurf-5-821-2017.

Thirumalai, K., Singh, A., & Ramesh, R. (2011). A MATLAB code to perform weighted linear regression with (correlated or uncorrelated) errors in bivariate data. *Journal of the Geological Society of India, 77*(4), 377-380. https://doi.org/10.1007/s12594-011-0044-1.

Trappitsch, R., Boehnke, P., Stephan, T., Telus, M., Savina, M. R., Pardo, O., et al., (2018). New constraints on the abundance of 60Fe in the early solar system. *The Astrophysical Journal Letters, 857*(2), L15. https://doi.org/10.3847/2041-8213/aabba9.

York, D., Evensen, N. M., Martınez, M. L., & De Basabe Delgado, J. (2004). Unified equations for the slope, intercept, and standard errors of the best straight line. *American Journal of Physics*, 72(3), 367-375. https://doi.org/10.1119/1.1632486

Figures and Captions

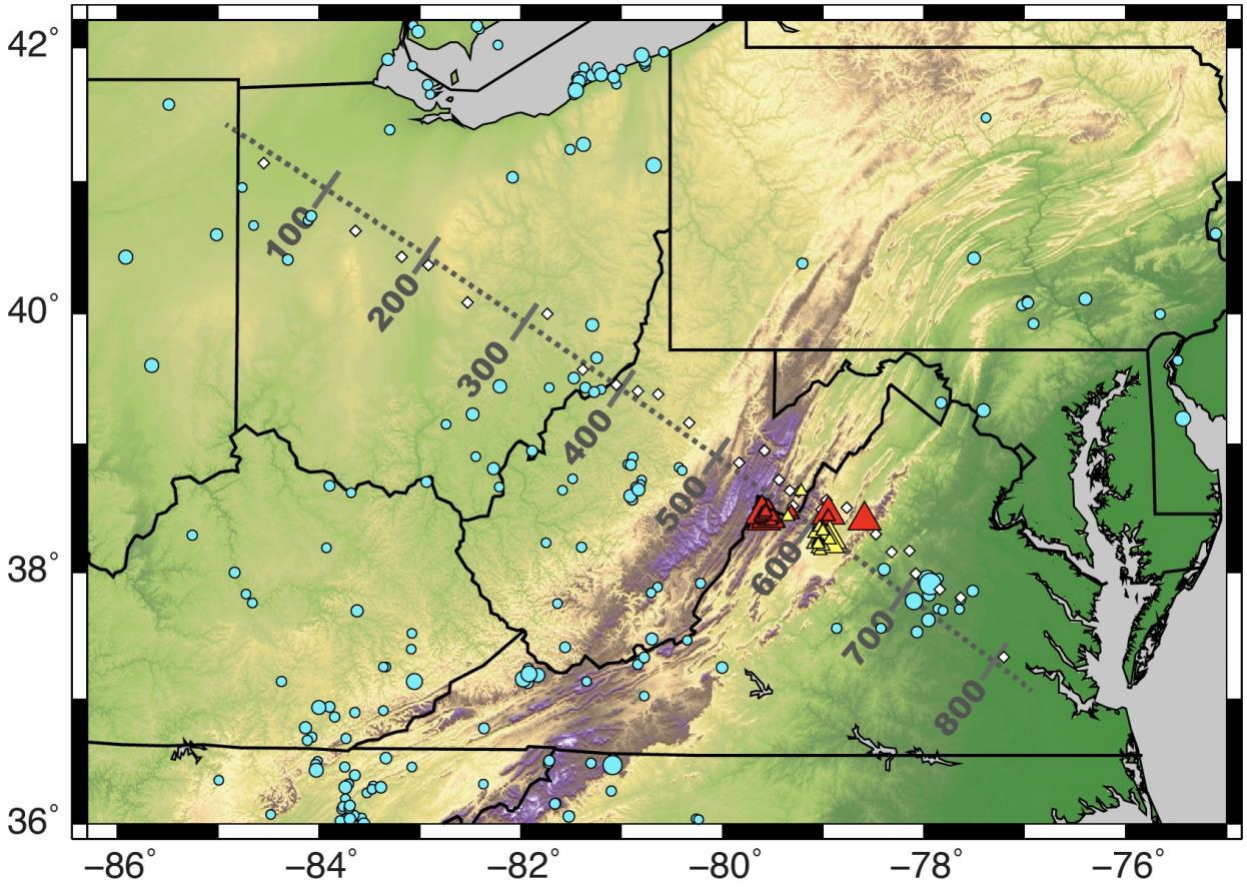

Figure 1. Map of study area. Background color shows topography. Triangle show locations of post-CAMP volcanism (Mazza et al., 2017). Larger triangles are samples with age constraints. Red triangles are Eocene, yellow triangles are Jurassic. Blue circles indicate seismicity from the NEIC catalog, 2001-2021 with M>2.5. Grey dotted line indicates location of cross-section shown in Figures 2 and 3. Tick marks show 100 km increments along that profile from NW to SE. White diamonds show locations of MAGIC stations.

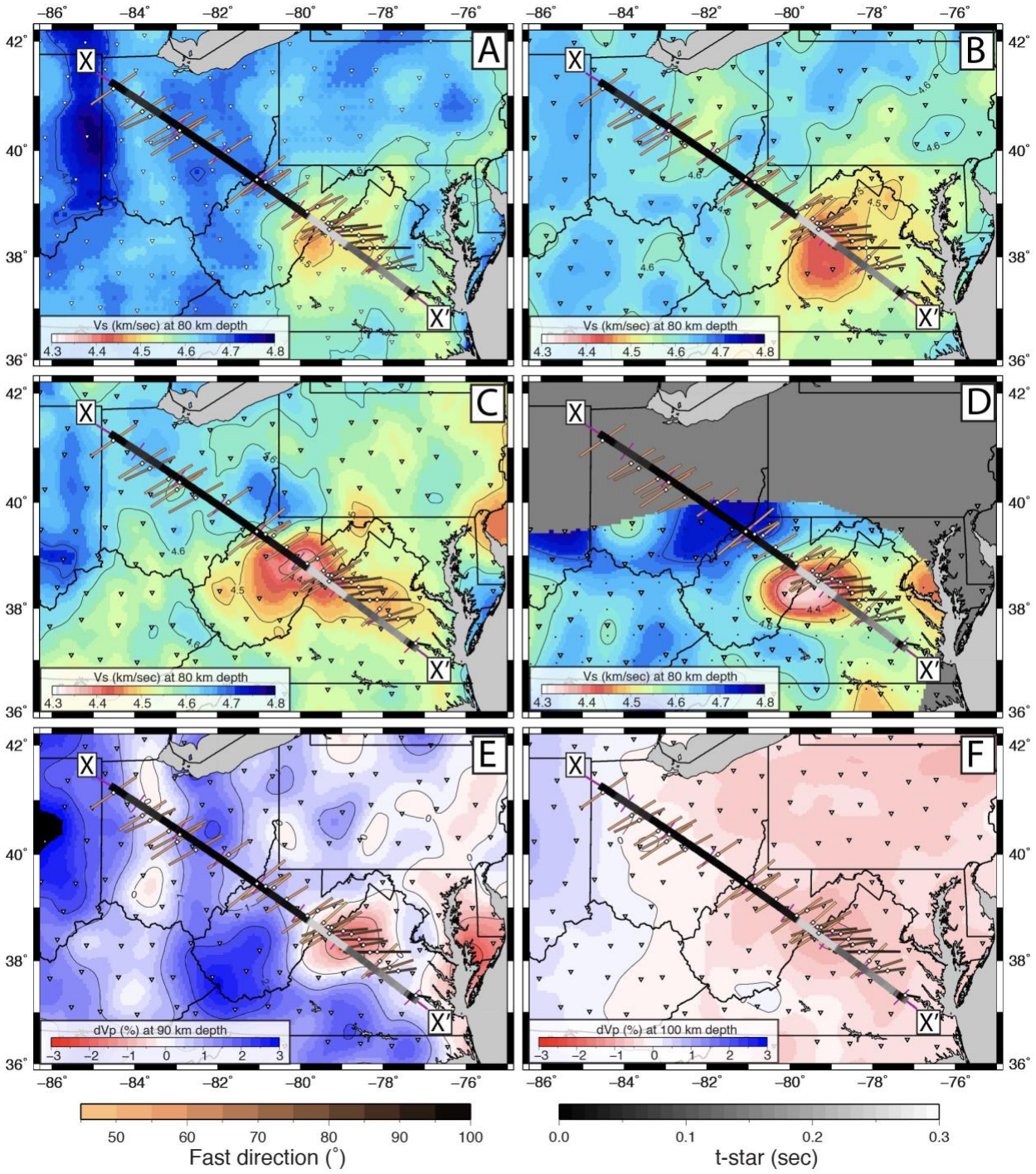

1738

1739 **Figure 2:** Seismic constraints on upper mantle structure in map view. Background colors show

1740 different tomographic models. A-D show absolute shear wave velocities from surface wave studies

1741 at 80 km depth, contoured at 0.1 km/sec: A) Schmandt et al. (2015); B) Shen & Ritzwoller, (2016);

1742 C) Porter et al. (2016); D) Wagner et al. (2018). Panels E & F show P-wave velocity deviations

determined from teleseismic travel time residuals contoured every 1% increment: E) at 90 km depth by Schmandt & Lin (2014); F) at 100 km depth by Boyce et al. (2019). Triangles show locations of EarthScope Transportable Array stations. For D) only stations used in the inversion are shown. Small black dots in D) show inversion grid node locations. Transect X-X' shown in purple with purple tick marks every 100 km from N-S shows location of the cross section in Figure 3. Superimposed on the transect is the projection of t* measurements from Byrnes et al. (2019). SKS splitting measurements from Aragon et al. (2017) at MAGIC stations (diamonds) are shown as bars color coded by fast direction in degrees clockwise from north.

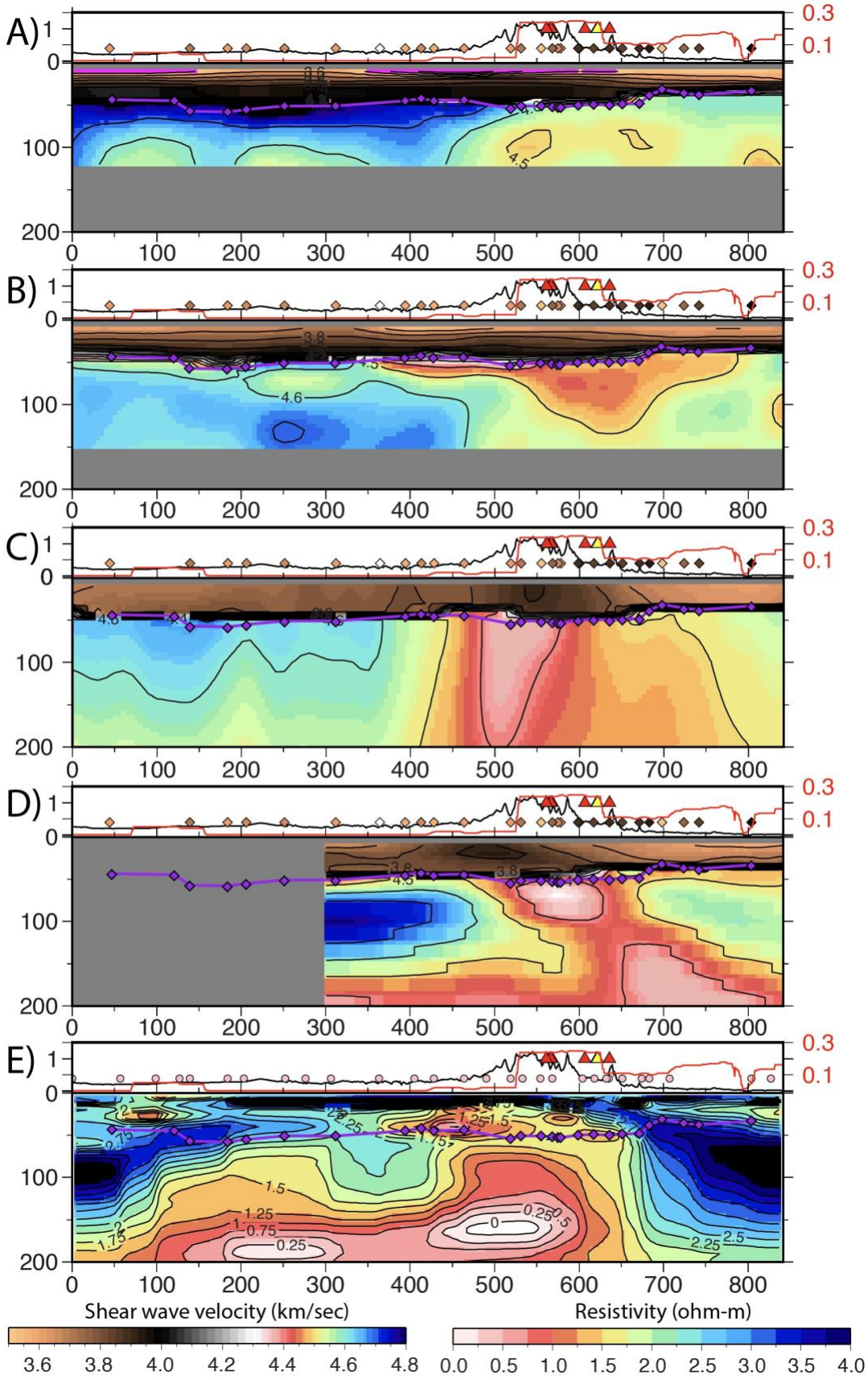
A)
B)
C)
D)
E)
0.3
0.1
0
100
200
0
100
200
300
400
500
600
700
800
Shear wave velocity (km/sec)
3.6
3.8
4.0
4.2
4.4
4.6
4.8
Resistivity (ohm-m)
0.0
0.5
1.0
1.5
2.0
2.5
3.0
3.5
4.0

1751

Figure 3: Cross-sections along X-X' as shown in Figure 2. At the top of each panel, black line shows topography, red line shows t* measurements of Byrnes et al. (2019), red triangles show the locations of Eocene volcanism, and yellow triangle shows Jurassic volcanism (Mazza et al., 2017). In Panels A-D, diamonds show projected locations of MAGIC stations color coded by fast splitting directions using the same color scale used in Figure 2. Panel E shows the locations of MT stations used in Evans et al. (2019). Models A-D correspond to the same seismic velocity models in A-D in Figure 2: A) Schmandt et al. (2015); B) Shen & Ritzwoller (2016); C) Porter et al. (2016); D) Wagner et al. (2018). Colors show shear wave velocities in km/sec. Panel E shows the electrical resistivity model of Evans et al. (2019). In all panels, purple line and purple diamonds show estimates of Moho depths determined from Ps receiver function analysis from Long et al. (2019).

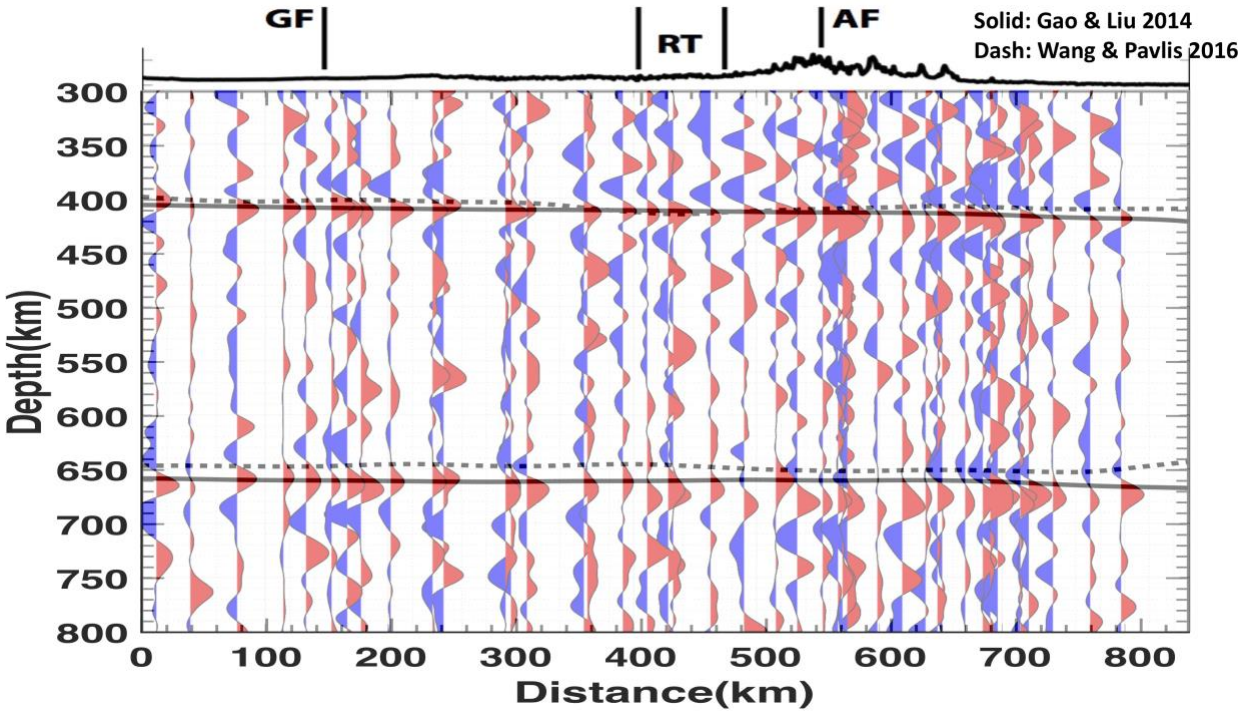

Figure 4. Image of Ps conversions from transition zone discontinuities beneath the MAGIC line (Liu et al., 2018). Radial component Ps receiver function traces have been stacked at individual stations, migrated to depth using a standard Earth model (iasp91; Kennett & Engdahl, 1991), and plotted as a function of distance along the MAGIC profile (as shown in Figure 1). Red pulses indicate a conversion due to a discontinuity with a positive velocity gradient, as expected for the 410 and 660 km discontinuities. Liu et al. (2018) observed a generally constant transition zone thickness across the MAGIC line, consistent with imaging by Gao and Liu (2014; solid line) and Pavlis et al. (2016; dashed line) using data from TA stations.

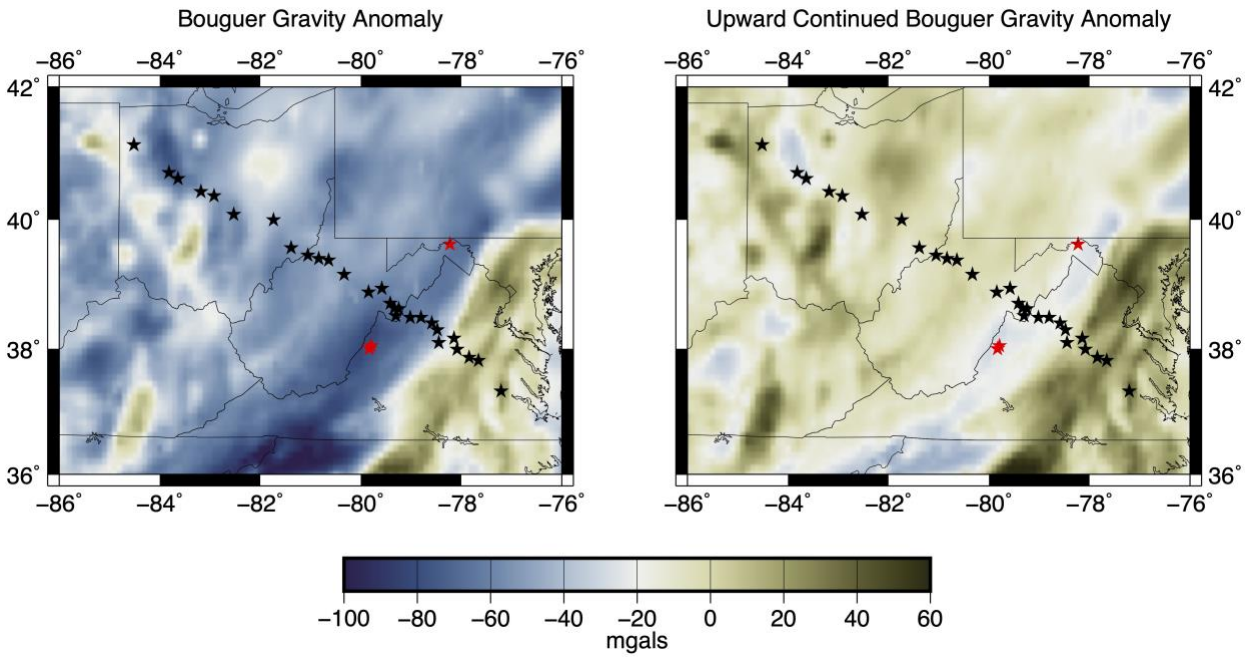

Figure 5. Gravity anomaly maps of the Central Appalachians. Left panel shows Bouguer gravity anomaly from PACES, while right panel shows a reduced Bouguer gravity anomaly map obtained following Stein et al. (2014). We upward continued the Bouguer anomaly data to 40 km and subtracted the result from the original Bouguer anomaly data. Black stars show the locations of MAGIC stations, while red stars show locations of prominent hot springs.

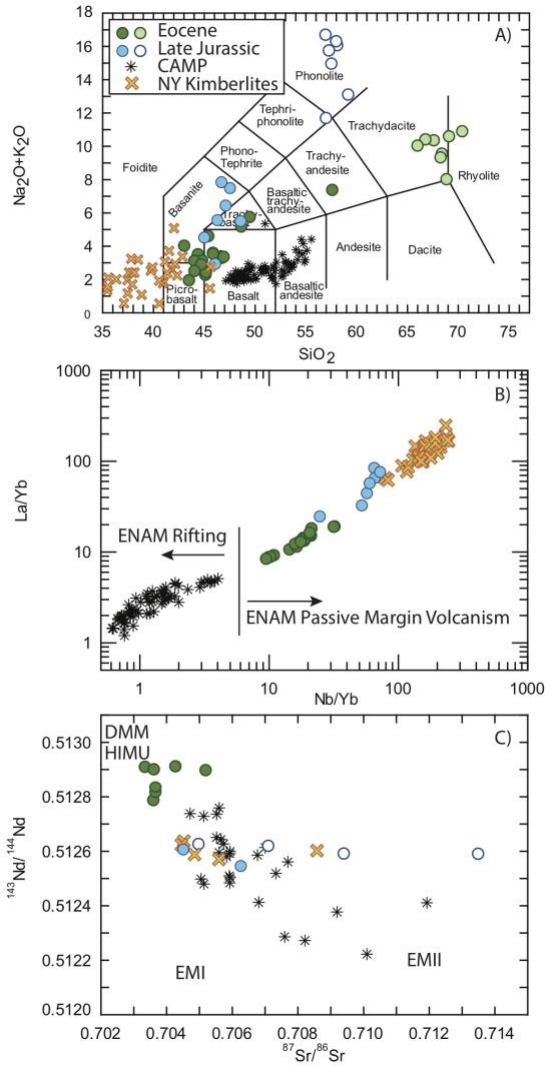

1784

1785 Figure 6. A) Total alkalis (Na_2O v+ K_2O) versus SiO_2 for the eastern North American Margin
1786 (ENAM) volcanics including the Virginia-West Virginia Late Jurassic and Eocene volcanic pulses
1787 showing bimodal populations (Mazza et al., 2014, 2017), the Central Atlantic Magmatic Province
1788 (CAMP, Callegaro et al., 2013; Whalen et al., 2015), and the New York (NY) kimberlites (Bailey
1789 & Lupulescu, 2015). B) La/Yb versus Nb/Yb showing differences in eastern North American
1790 Margin (ENAM) rifting and passive margin volcanics. C) $^{143}Nd/^{144}Nd$ versus $^{87}Sr/^{86}Sr$ for ENAM
1791 volcanics. DMM – depleted MORB mantle, EMI – enriched mantle I, EMII- enriched mantle II,
1792 HIMU – high $^{238}U/^{204}Pb$ mantle.

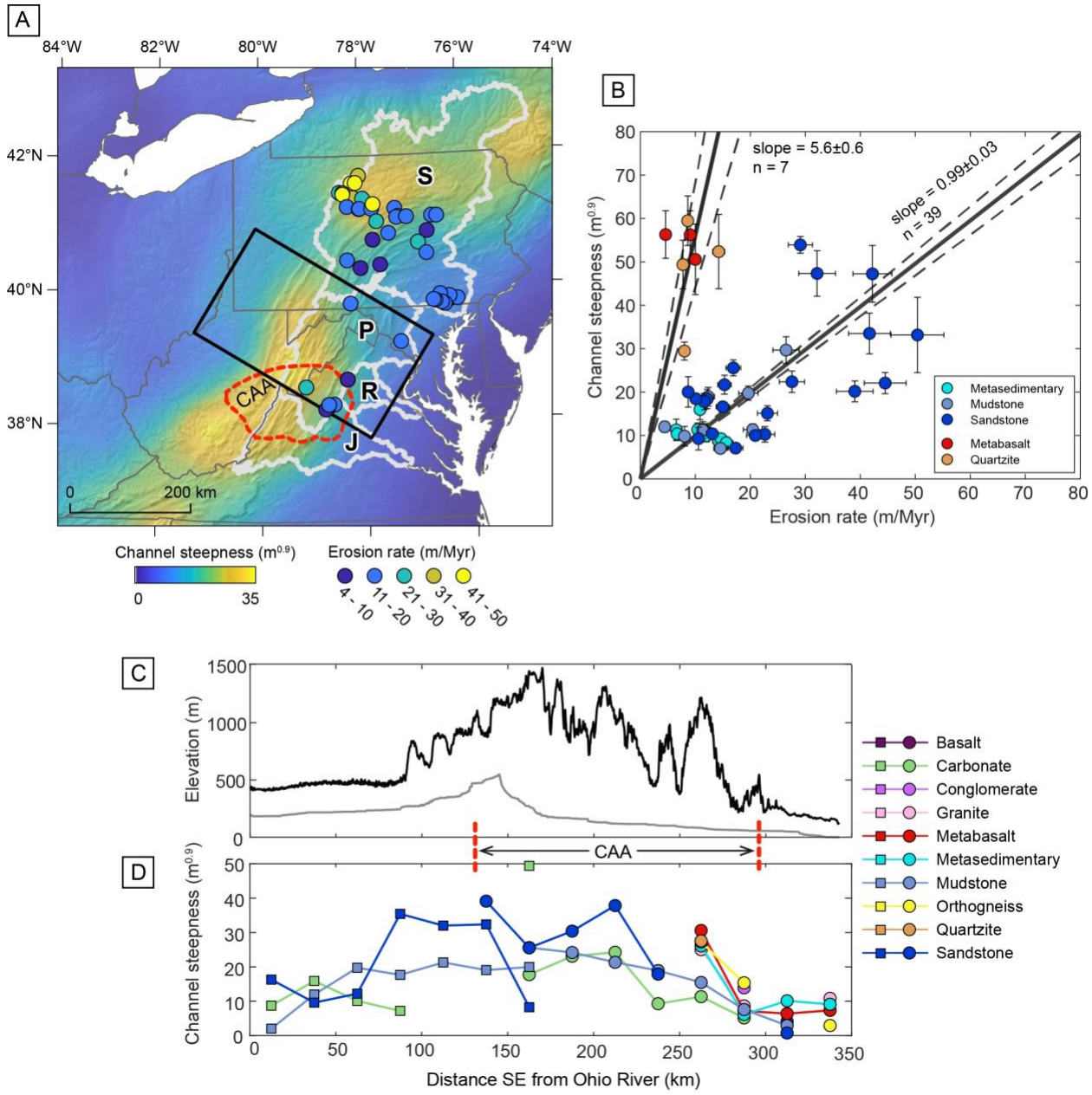

1793

1794 Figure 7. Topography and erosion rates in the Central Appalachians. A.) Map of study area
1795 showing smoothed channel steepness indices throughout study area. Red dashed line shows the
1796 approximate outline of the CAA based on the 4.5 km/s contour in Wagner et al., 2018 (see Figure
1797 2D), and black rectangle outlines the swath profiles shown in C and D. Colored circles represent
1798 locations of erosion rate samples used in the analysis (see text for details). Watershed boundaries
1799 of major rivers shown in white; J-James, R-Rappahannock, P-Potomac, S-Susquehanna. B.)

Scaling relationships among channel steepness, erosion rate, and lithology for basins throughout the central Appalachian region. Results of York regressions forced through origin characterize two separate groups of rock type; 2σ bounds shown with dashed lines. C.) Maximum (black) and minimum (gray) elevations along the swath profile. D.) Mean values of channel steepness along the swath profile separated by rock type and drainage direction. Channels west of the drainage divide are shown with square symbols, and channels east of the divide are shown with circles.

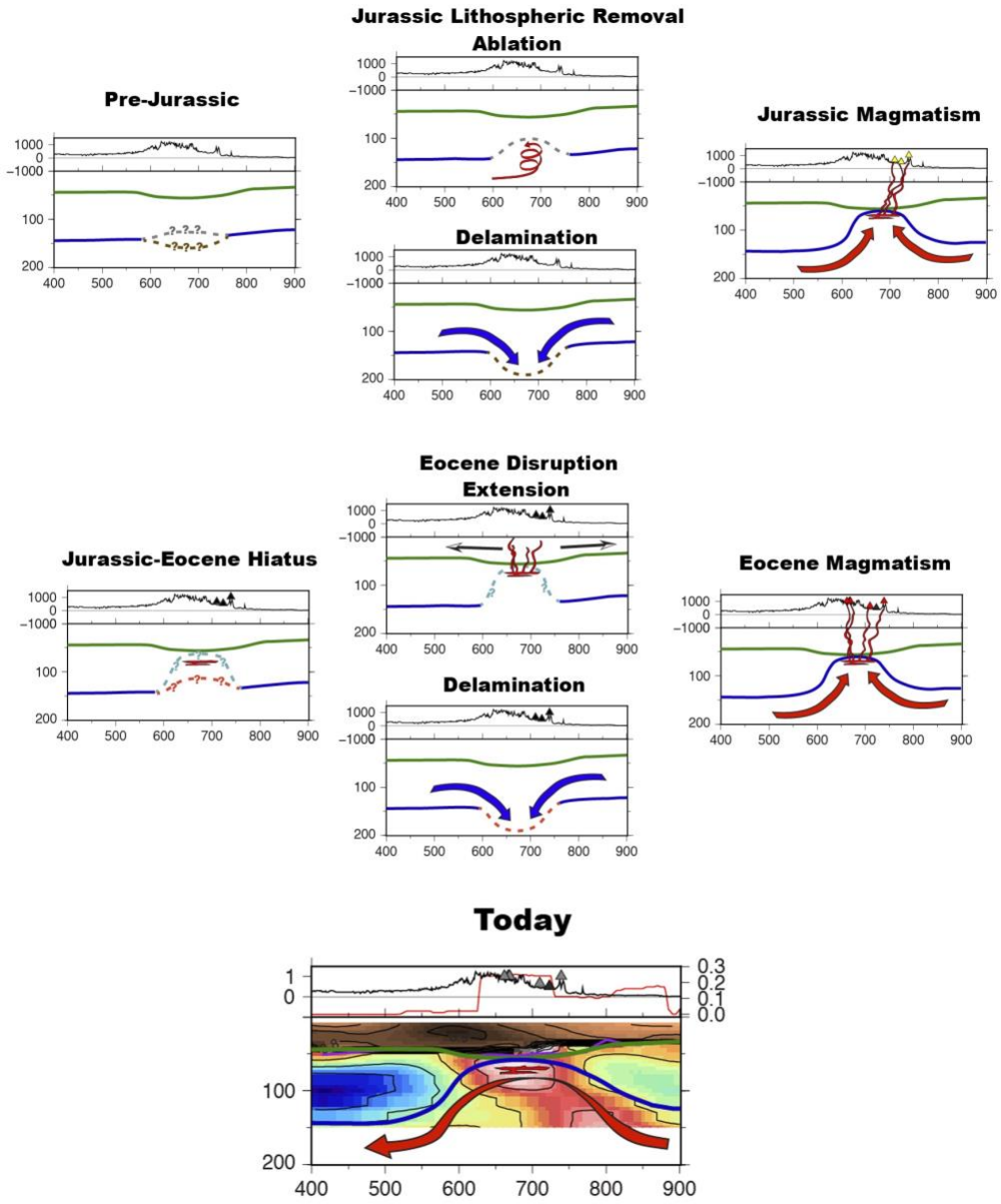

1807

1808 Figure 8. Schematic cartoon of possible scenarios for lithospheric removal and evolution from the
1809 Jurassic to the present. Top set of panels shows possible configurations and processes during the
1810 Jurassic (including pre-removal, during lithospheric removal, and during magmatism), middle set
1811 of panels shows possible configurations and processes during the Eocene (including during the

Jurassic-Eocene hiatus, during lithospheric removal, and during magmatism), and the bottom panel shows the present-day configuration. In all panels, the green line indicates the possible Moho architecture and the blue line indicates the possible LAB geometry; lines are dashed where uncertainty is particularly high. Red colors indicate the likely presence of melt, arrows indicate possible (highly schematic) flow scenarios, and triangles indicate magmatic products at surface. In the lower panel, plotting conventions and velocity models are as in Figure 3d. Present-day topography is shown at the top of all panels for reference.